UNIVERSITY OF THESSALY

DEPARTMENT OF MECHANICAL ENGINEERING

LABORATORY OF MECHANICS AND STRENGTH OF MATERIALS

Post-Graduate Diploma

FINITE ELEMENT SIMULATION OF UOE PIPE MANUFACTURING PROCESS AND ITS EFFECT ON OFFSHORE PIPELINE MECHANICAL BEHAVIOR

Giannoula Chatzopoulou

Diploma in Civil Engineering, University of Thessaly, 2012

Submitted to the Department of Mechanical Engineering

in Partial Fulfillment of the Requirements

for the Degree of Post-Graduate Diploma

Volos, 2014

ΠΑΝΕΠΙΣΤΗΜΙΟ ΘΕΣΣΑΛΙΑΣ
ΠΟΛΥΤΕΧΝΙΚΗ ΣΧΟΛΗ
ΤΜΗΜΑ ΜΗΧΑΝΟΛΟΓΩΝ ΜΗΧΑΝΙΚΩΝ

Μεταπτυχιακή Εργασία

ΑΝΑΛΥΣΗ ΠΕΠΕΡΑΣΜΕΝΩΝ ΣΤΟΙΧΕΙΩΝ ΤΗΣ ΚΑΤΕΡΓΑΣΙΑΣ ΠΑΡΑΓΩΓΗΣ ΣΩΛΗΝΩΝ UOE ΚΑΙ ΤΗΣ ΕΠΙΡΡΟΗΣ ΣΤΗ ΜΗΧΑΝΙΚΗ ΣΥΜΠΕΡΙΦΟΡΑ ΥΠΟΘΑΛΑΣΣΙΩΝ ΑΓΩΓΩΝ

υπό

ΓΙΑΝΝΟΥΛΑ ΧΑΤΖΟΠΟΥΛΟΥ

Διπλωματούχου Πολιτικού Μηχανικού Π.Θ., 2012

Υπεβλήθη για την εκπλήρωση μέρους των
απαιτήσεων για την απόκτηση του
Μεταπτυχιακού Διπλώματος Ειδίκευσης

Βόλος, 2014

Εγκρίθηκε από τα Μέλη της Τριμελούς Εξεταστικής Επιτροπής:

Πρώτος Εξεταστής (Επιβλέπων)	Δρ. Σπύρος Α. Καραμάνος Αναπληρωτής Καθηγητής, Τμήμα Μηχανολόγων Μηχανικών, Πανεπιστήμιο Θεσσαλίας
Δεύτερος Εξεταστής	Δρ. Αλέξιος Κερμανίδης Επίκουρος Καθηγητής, Τμήμα Μηχανολόγων Μηχανικών, Πανεπιστήμιο Θεσσαλίας
Τρίτος Εξεταστής	Δρ. Αντώνιος Γιαννακόπουλος Καθηγητής, Τμήμα Πολιτικών Μηχανικών, Πανεπιστήμιο Θεσσαλίας

FINITE ELEMENT SIMULATION OF UOE PIPE MANUFACTURING PROCESS AND ITS EFFECT ON OFFSHORE PIPELINE MECHANICAL BEHAVIOR

Giannoula Chatzopoulou

Department of Mechanical Engineering

University of Thessaly, Volos, Greece

Advisor: Dr. S.A. Karamanos

Keywords: UOE forming process, steel pipes, finite elements, buckling.

Abstract. *A significant number of large-diameter-thickness line pipes used in offshore applications are commonly manufactured by cold-forming plates through the UOE process, consisting of four sequential forming steps. In this thesis, the UOE forming process is modeled numerically through the application of a non-linear finite element program, and focuses on the effect of the manufacturing process on the buckling pressure and the bending capacity of the offshore pipeline. Special emphasis is given on the constitutive model for the accurate description of inelastic steel behavior due to reverse plastic loading; a special-purpose model is developed, based on nonlinear kinematic hardening, capable of describing the plastic plateau at initial yielding of the steel plate, as well as the Bauschinger effect. In addition, a parametric analysis is also conducted focusing on the effects of line pipe expansion on the structural capacity of the pipe.*

ΑΝΑΛΥΣΗ ΠΕΠΕΡΑΣΜΕΝΩΝ ΣΤΟΙΧΕΙΩΝ ΤΗΣ ΚΑΤΕΡΓΑΣΙΑΣ ΠΑΡΑΓΩΓΗΣ ΣΩΛΗΝΩΝ UOE ΚΑΙ ΤΗΣ ΕΠΙΡΡΟΗΣ ΣΤΗ ΜΗΧΑΝΙΚΗ ΣΥΜΠΕΡΙΦΟΡΑ ΥΠΟΘΑΛΑΣΣΙΩΝ ΑΓΩΓΩΝ

Γιαννούλα Χατζοπούλου

Τμήμα Μηχανολόγων Μηχανικών

Πανεπιστήμιο Θεσσαλίας

Επιβλέπων Δρ. Σπύρος Α. Καραμάνος

Περίληψη. *Μεγάλης διαμέτρου αγωγοί από χάλυβα που χρησιμοποιούνται σε υπεράκτιες (υποθαλάσσιες) εφαρμογές, συνήθως κατασκευάζονται με εν ψυχρώ διαμόρφωση από επίπεδα ελάσματα μέσω της κατεργασίας UOE, η οποία αποτελείται από τέσσερα μηχανικά βήματα. Στην παρούσα εργασία, η κατεργασία UOE προσομοιάζεται αριθμητικά, μέσω μη-γραμμικής ανάλυσης πεπερασμένων στοιχείων και επικεντρώνεται στην επίδραση της εν λόγω κατεργασίας στην αντοχή σε εξωτερική πίεση και στην αντοχή σε κάμψη με παρουσία εξωτερικής πίεσης. Ιδιαίτερη έμφαση δίνεται στο καταστατικό μοντέλο του υλικού που περιγράφει την ανελαστική συμπεριφορά λόγω πλαστικής φόρτισης αντίθετης διεύθυνση. Το μοντέλο αυτό περιγράφει τη μη γραμμική κινηματική κράτυνση και είναι ικανό να περιγράψει την περιοχή του πλαστικού πλατώ καθώς και το φαινόμενο Bauschinger. Επιπροσθέτως μια παραμετρική ανάλυση διεξάγεται και εστιάζει στην επίδραση της διαστολής (expansion) στην αντοχή του αγωγού σε εξωτερική πίεση και στην αντοχή του σε κάμψη με παρουσία εξωτερικής πίεσης.*

Tableof Contents

Table of Figures

1 Introduction

Oil and gas pipelines are widely used in transporting hydrocarbon energy resources in the most effective and safe way. Pipelines usually require a significant initial investment cost for their manufacturing, but during their service life (30-40 years) they have relatively low maintenance and operational costs; they are also characterized by a small number of accidents. In recent years a considerable number of pipelines has been constructed or are in the design stage. In addition several important pipeline projects are in the planning stage, which quite often connect different countries or different continents (e.g. Europe – Asia, Europe – Africa). In some cases, a long segment of the pipeline is underwater. The current technological know-how allows for the installation of such pipes in water depths exceeding 2000 m. For example the Blue Stream gas pipeline that connects Russia and Turkey through the Black Sea at depths that reach 2.200m, whereas the state-of- the art design of offshore pipelines refers the Oman-India pipeline at depths that reach 3.500m. [1]).

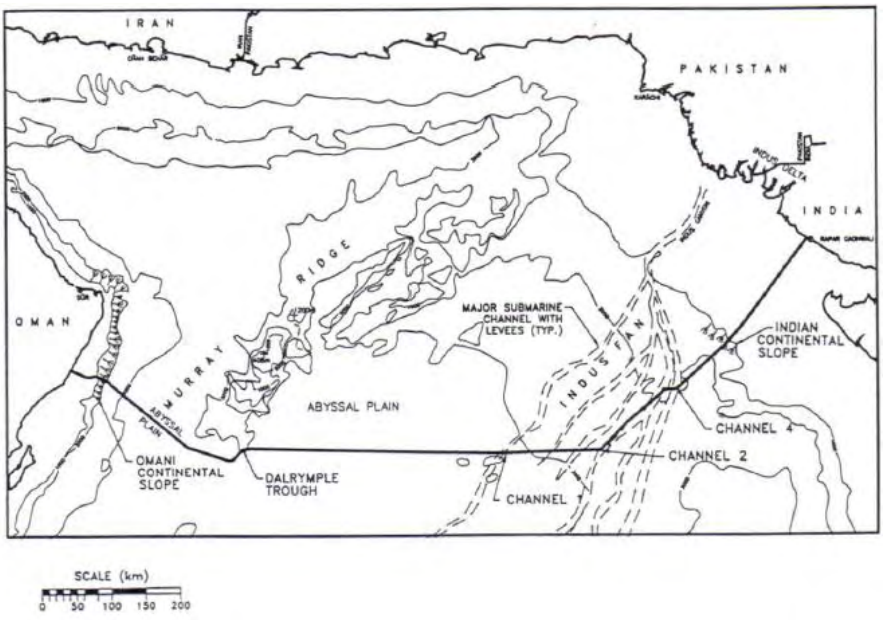

Figure 1: Oman-India Pipeline alignment.

1.1 Externally pressurized pipes

The mechanical design of offshore pipelines, according to the modern design concept, is based on the limit-state design approach. Following this philosophy, one should design the pipeline against all possible failure modes. Buckling under external pressure constitutes a fundamental limit state for the design of offshore pipelines. The external pressure is due to the significant water depth and the corresponding failure is commonly mentioned as “collapse” (Langner [2], Yeh and Kyriakides [3], Karamanos and Tassoulas [4]), associated with a flattened “dog-bone” shape of the pipe cross-section. In order to resist high levels of external pressure in water depths that exceed 2000m, deep-water pipelines are thick-walled with a diameter-to-thickness ratio less than 25.

The external pressure capacity of thick-walled pipelines has been studied in numerous publications (Yeh and Kyriakides [3], Kyriakides and Yeh [5], Al-Sharif and Preston[6], Baek [7], Benjamin and Cunha [8], DeGeer and Cheng [9], Guarracino et al.[10], Haagsma and Schaap [11], Murphey and Langner [12], Tsuru and Asahi [13]). In those publications, it was recognized that thick walled pipelines fail at a pressure level close to the nominal yield pressure of the pipe cross-section (P_0)

$$P_0 = 2\sigma_y \frac{t}{D_m} \tag{1.1}$$

where σ_y is the yield stress, t is the thickness of the pipe and D_m is the mean diameter of the pipe.

In addition, it was found that the value of the ultimate pressure is sensitive to the presence of initial imperfections such as ovality, eccentricity, material stress-strain behavior and residual stresses. The ovalization parameter is equal to Δ_0

$$\Delta_0 = \frac{|D_1 - D_2|}{D_1 + D_2} \tag{1.2}$$

where D_1 and D_2 are the horizontal and vertical outer diameters correspondingly

Two-dimensional numerical simulations have been conducted in the present study using the numerical finite element model described in later section. Two-dimensional can be adopted due to the low D/t ratios considered in the present study. More specifically, for low D/t rations, failures are expected to take place due to pipe ovalization is prior to the development of local buckles. Therefore, two-dimensional analysis is adequate for the simulation.. Figure 2 shows the response of an imperfect pipe with diameter and thickness equal to 606.24 mm and 32.3 mm respectively, in the presence of initial imperfections. The steel material yield stress considered for the analysis is equal to $\sigma_y = 460MPa$. Initial imperfection is geometric, assumed in the form of a doubly-symmetric ovalization shape. The results of Figure 2 shows that there is a strong dependence of the maximum pressure and the amplitude of initial imperfection. Furthermore, Figure 3 the effects of residual stresses and initial imperfection on the external pressure capacity are shown. Residual stresses are assumed only in hoop direction of the pipe, neglecting residual stresses in the longitudinal direction, with a linear variation through the pipe thickness, with a maximum value equal to $\sigma_y / 2$. For small values of initial imperfections, residual stresses have a certain effect on the value of the ultimate pressure. This effect becomes negligible for large values of initial imperfection amplitude.

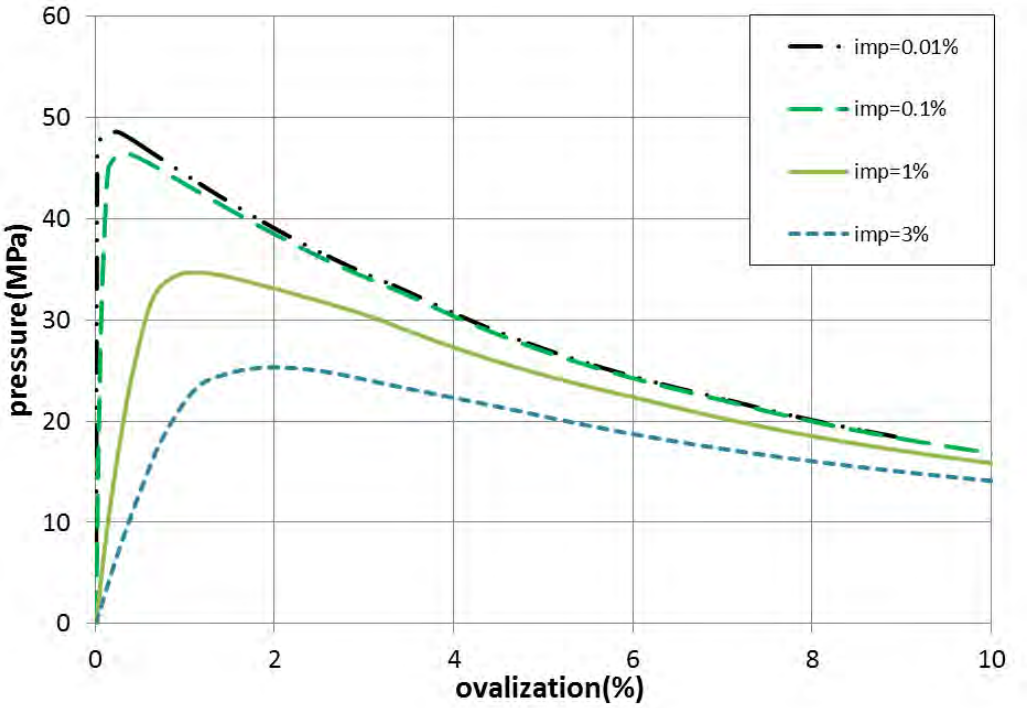

Figure 2: The response of an imperfect pipe under external pressure for different amplitudes of initial imperfections.

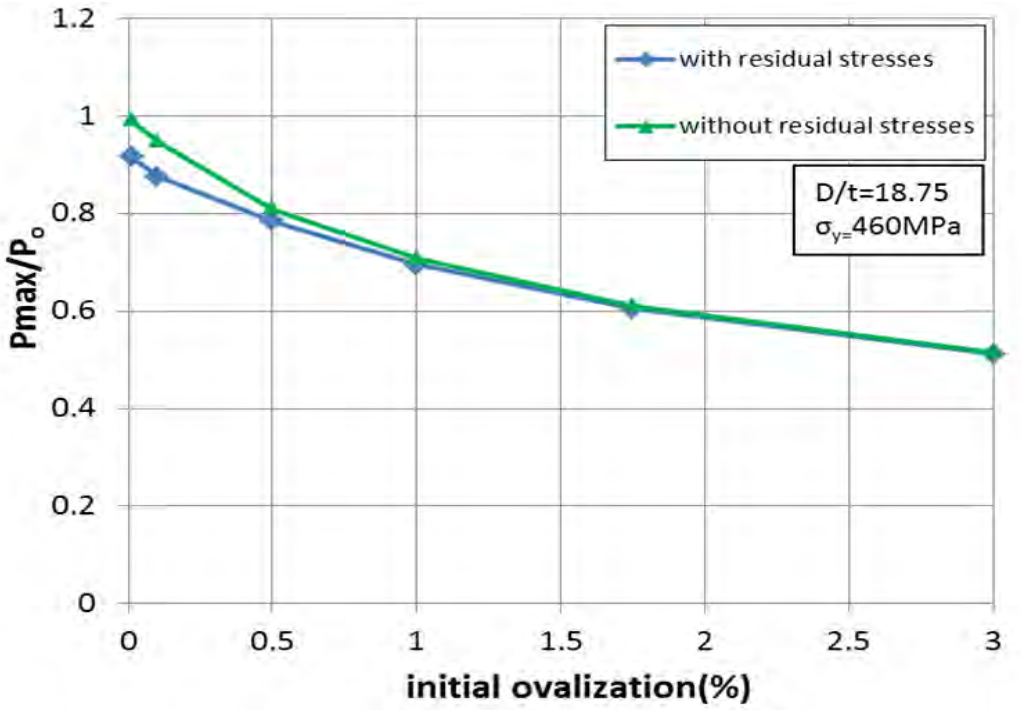

Figure 3: The effects of residual stresses and initial ovalization on the pipe pressure capacity.

1.2 Bending loads in the presence of external pressure

The pipeline may also undergo significant bending loads in the presence of high external pressure during its installation and operation stages (Corona and Kyriakides [14] Karamanos and Tassoulas [4]). In those studies, it has been recognized that the value of the curvature $k_{\max}$, at which maximum moment occurs, is sensitive to the presence of initial imperfections and residual stresses. Figure 4 shows the response of an imperfect pipe with diameter and thickness equal to 606.24 mm and 32.3 mm respectively, in the presence of initial imperfections and residual stresses, yield stress is equal to $\sigma_y = 460MPa$ as well. Initial imperfection is assumed in the form of a doubly-symmetric ovalization shape. The results of Figure 4 refer to the bending capacity with the presence of constant external pressure, equal to 20MPa, and show the effect of the initial imperfection amplitude and the effect of residual stresses on curvature $k_{\max}$ corresponding to the maximum moment that the pipe under consideration is able to sustain. The values of curvature are normalized by the following curvature parameter $k_1 = t / D_m$. It is observed that for small values of initial imperfections, residual stresses have a certain effect on the value of the curvature $k_{\max}$, while this effect becomes negligible for large values of initial imperfection amplitude.

Moreover, a comparison with experimental results on stainless steel (SS-304) pipes with D/t equal to 19.2 and ovalization Δ_0 equal to 0.05% has been conducted in order to examined the reliability of the models, the experimental results can be found in [14]. Results (Figure 5) show $P \to k$ path from experimental results and 2D simulation with the same geometric and material parameters. The figure illustrates that is good agreement of numerical results with the available experimental data.

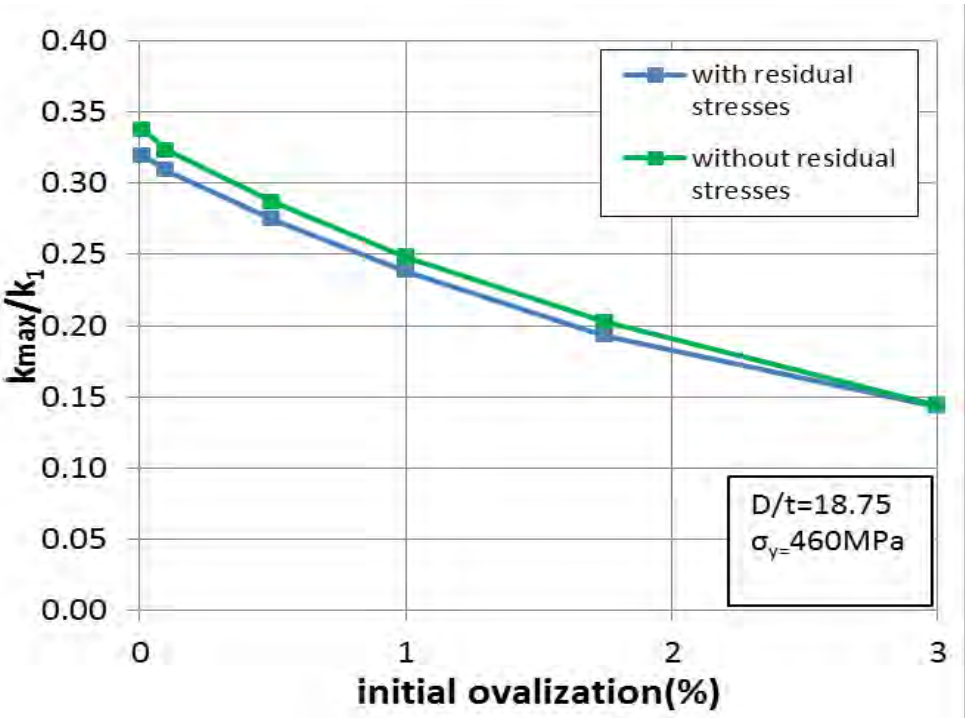

Figure 4: The effects of residual stresses for a pipe subjected to constant external pressure $P/P_0 = 0.40$.

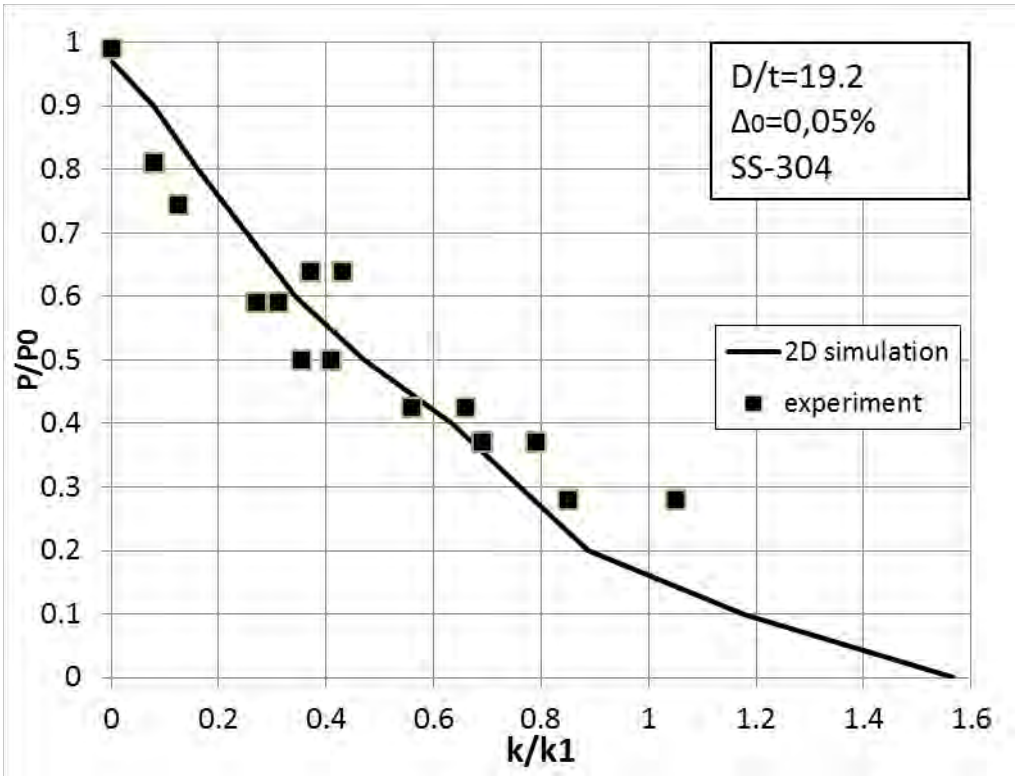

Figure 5: Experimental and predicted collapse envelope for tubes with *D/t=19.2*

1.3 The UOE forming process

The UOE manufacturing process is a commonly adopted method for manufacturing thick-walled steel line pipes for deep water applications. The forming process is important in determining the level of imperfections and residual stresses in a line pipe, and therefore, it should be taken into consideration for the prediction of the ultimate external pressure and pressurized bending capacity (Gresnigt and Van Foeken [15]). In the present study, the UOE cold-forming manufacturing process is examined in terms of its effects on the mechanical behavior of offshore pipelines. An initial study on the effects of the UOE process has been reported by Kyriakides et al. [16] using a simple analytical model. A recent finite element study has been reported on the effect of UOE process on the collapse pressure by Herynk et al.[17] who employed an advanced two-surface plasticity model. Additional publications have been reported by Toscano et al. [18] and Varelis et al. [19] on the ultimate pressure capacity of UOE pipes, using finite element models and more traditional plasticity models. Those studies have shown the influence of this manufacturing process on the value of the collapse pressure. However, to the author's knowledge, the effects of UOE manufacturing process on the pressurized bending response of pipelines has not been examined.

1.4 Scope of the present study

In the present study, the UOE forming process for a 24-inch, $D/t = 18.85$, pipeline, candidate for deep-water applications, is simulated using a rigorous two-dimensional finite elements, so that initial imperfections and residual stresses at the end of the manufacturing process are predicted with a high degree of accuracy. The pipe under consideration is similar to one considered in [17]. Subsequently, considering the final state of the UOE line pipe, its structural behavior is examined under combined bending and external pressure to determine

its collapse pressure and its bending response under pressurized conditions. Moreover, a comparison in structural behavior between UOE pipes and Seamless pipes is conducted. To model steel material behavior, an efficient cyclic plasticity material model is developed, based on nonlinear kinematic hardening, capable of describing both the yield plateau region of the steel stress-strain curve and the Bauschinger effect under reverse plastic loading. Simulation of the manufacturing process results in determining residual stresses and deformations within the line pipe, as well as line pipe geometry (ovality and thickness). Moreover, a short parametric analysis is conducted focusing on the effects of the amount of expansion (the final stage of the UOE process) on the structural capacity of the pipe. The developed numerical model can be employed for optimizing the UOE manufacturing process, in terms of increasing the ultimate capacity of the offshore pipeline under external pressure and bending. Finally, the bending response of UOE pipes under pressurized conditions is also examined with a simplified methodology.

2 Description of the UOE manufacturing process

A popular manufacturing method for large diameter pipes used in subsea consists of cold-forming long plates through the UOE process. The name UOE stems from the initials of the last three of these mechanical steps (**U**-ing, **O**-ing, **E**-xpansion). The UOE steel pipe forming process was originally proposed for underground (buried) pipes, but recently it has been extended to subsea pipes. Nowadays, it is considered a very common method of thick walled line pipe production.

The process starts with a wide steel plate, and the line pipe is formed in four sequential mechanical steps (phases) as shown in Figure 6:

(a) Crimping of the plate edges

(b) U-ing: the pipe is formed into a U-shape

(c) O-ing: the pipe is pressed into an almost circular shape and both ends of the plate are welded and

(d) Expansion: the application of internal pressure for improving the “circular” shape of the pipe cross-section

The steps mentioned above are described in detail subsequently. The UOE process starts by trimming the longitudinal edges of the plate by milling so as to accommodate the welding. The first forming step involves crimping of the plate edges at both sides into circular arcs of about one radius width. This is achieved by pressing the ends between two shaped dies as shown in Figure 7. Because of the large forces required in this step, the forming is executed in several consequent stages. The length of the plate varies between one and four times the pipe diameter, depending on the pipe thickness. Each production factory is equipped with several sets of dies in order to adjust the forming process to the desired thickness and diameter of the pipes required. In particular, for a given pipe, the dies with the most appropriate inner and

outer radii (ρ_{Cri} and ρ_{CRo}) are selected, as depicted in Figure 7(b). The relative horizontal positions of the dies can be adjusted as desired. The width of the steel plate to be crimped is defined from the horizontal position of the dies (L_{CR}) and depends on the plate thickness and the maximum load capacity F_{CR} of the press (Figure 7(b)).

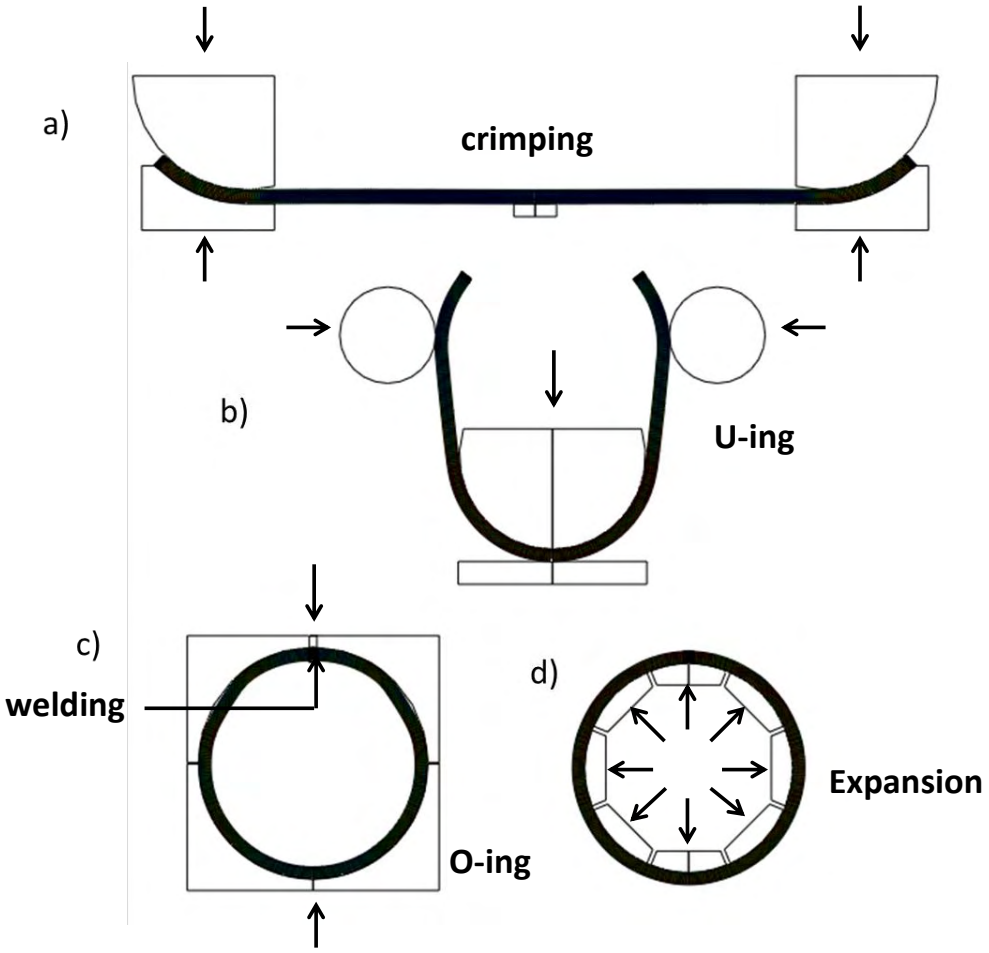

Figure 6: Schematic representation and main parameters of UOE forming steps: a) Crimping press, b) U-press, c) O-press, d) Expansion.

.

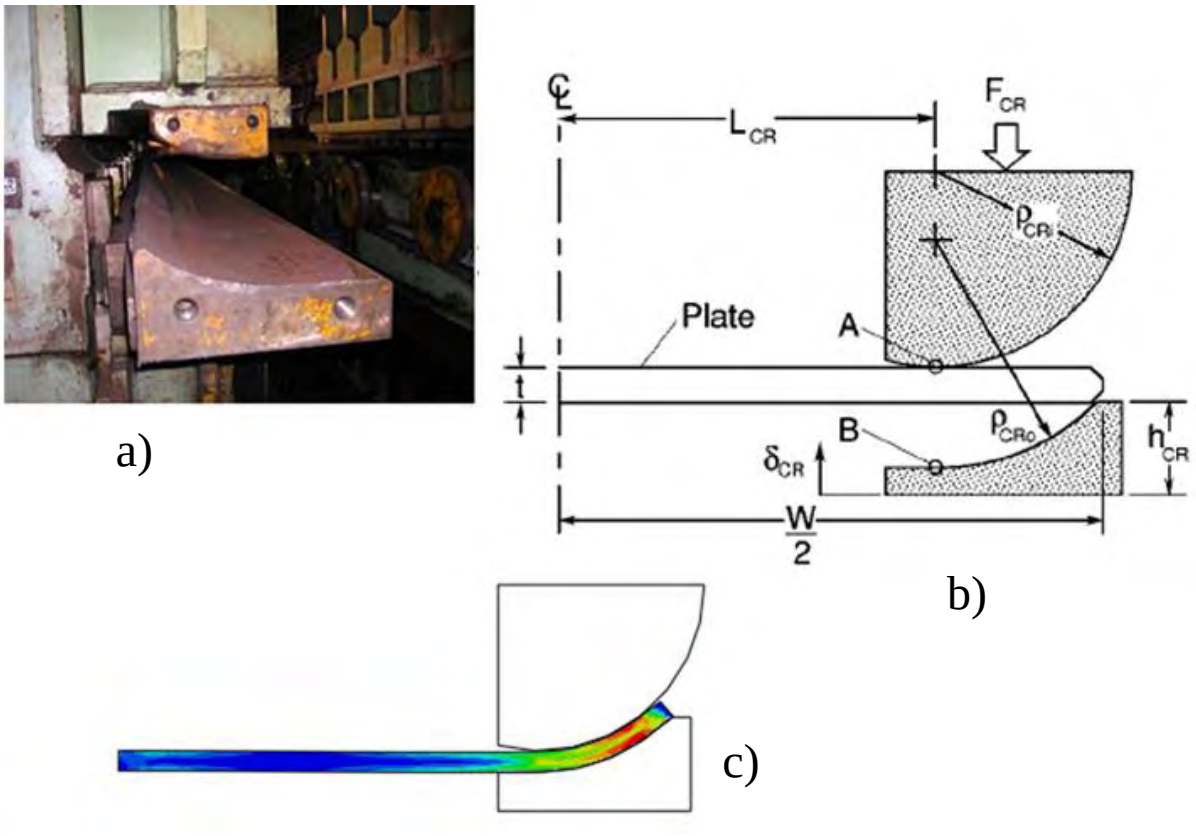

Figure 7: Crimping phase of UOE pipe forming: the lower die moves upwards; (a) representative phase of the forming process; (b) schematic representation of crimping press [17]; and (c) present finite element numerical simulation.

a)

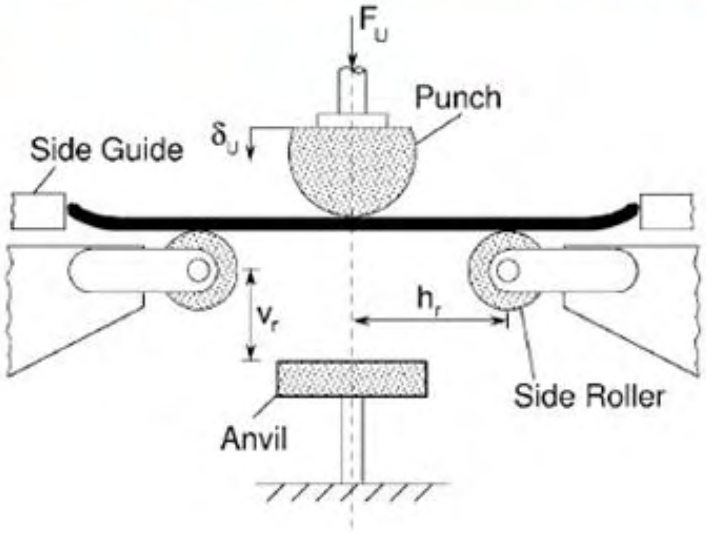

b)

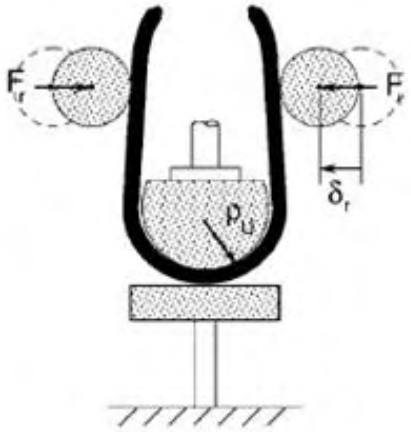

c)

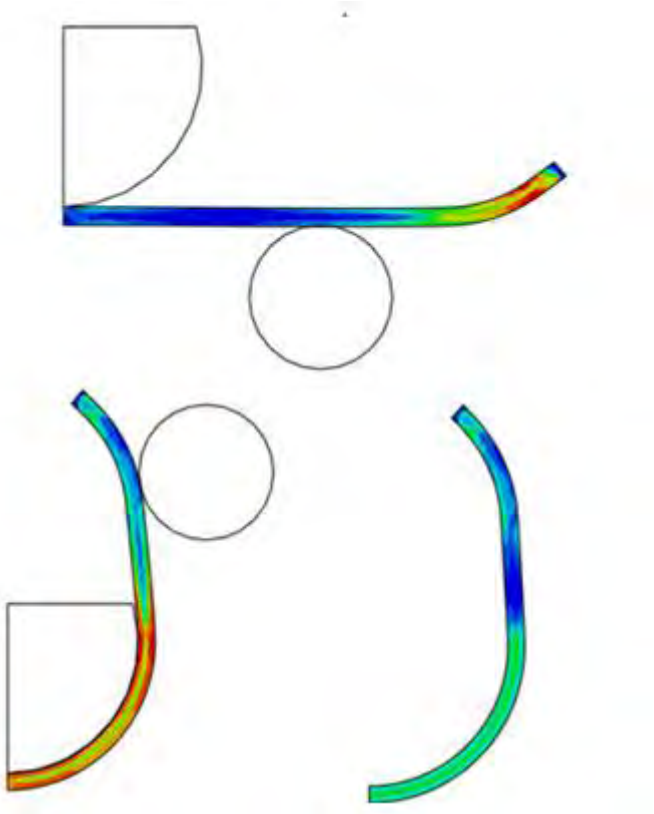

Figure 8: The U-ing phase is realized with the displacement of the U-punch, the displacement of the side rollers and the unloading of the steel; (a) photos for U-ing phase [18];(b)Schematic representation of U-ing process [17]; (c)numerical simulation at different stages during the U-ing phase.

Upon completion of this step, the steel plate proceeds to the U-ing phase (Figure 8). The U-ing step is performed in two stages. During the first stage, the U-punch moves downwards and bends the entire plate through a three-point bending process. The U-punch radius (ρ_U) is selected so that the lower half of the steel plate acquires a radius close to the desired pipe radius at the end of the step. The U-punch stops moving when the plate touches the anvil. The U-punch is then held in place, and the side rollers move inwards approaching one another. The horizontal position (h_r) where the side rollers are placed and the distance (δ_r) they cover are selected so that the final form of the plate to be close to a "U" shape and the two branches of the plate are nearly vertically positioned.

Subsequently, the plate is conveyed in the O-ing phase, which is realized by the approach of two semi-circular rigid dies with radius ρ_0. The upper die is pushed downwards, forcing the plate to acquire a circular form (Figure 9). The forming ends when the O-die covers the predefined displacement. After the O-ing phase, the two edges of the pipe already beveled from the initial phase are welded together with SAW (Submerged Arc Welding), first on the inside and then on the outside (Figure 12). At this stage, extensive ultrasonic checks are also performed to detect any defects prior to the pipe expansion.

The final step of the forming process is pipe expansion. This step is necessary to control the shape of the pipe cross-section so that welding between adjacent pipe segments is performed without significant misalignment. Furthermore, the expansion improves the roundness of the pipe giving it its final size, improving its structural performance in terms of ultimate buckling pressure. The step is realized through a mandrel which is inserted in the pipe (Figure 10). The mandrel may consist of 8, 10 or 12 segments. In the present study 8 segments were assumed in the circumference of the pipe. These segments are selected so that their radius (ρ_E) is almost equal to the internal radius of the pipe. The mandrel is hydraulically actuated and all the segments move outwards radially. The distance covered by the segments depends on the plate thickness and constitutes a basic parameter of the manufacturing process.

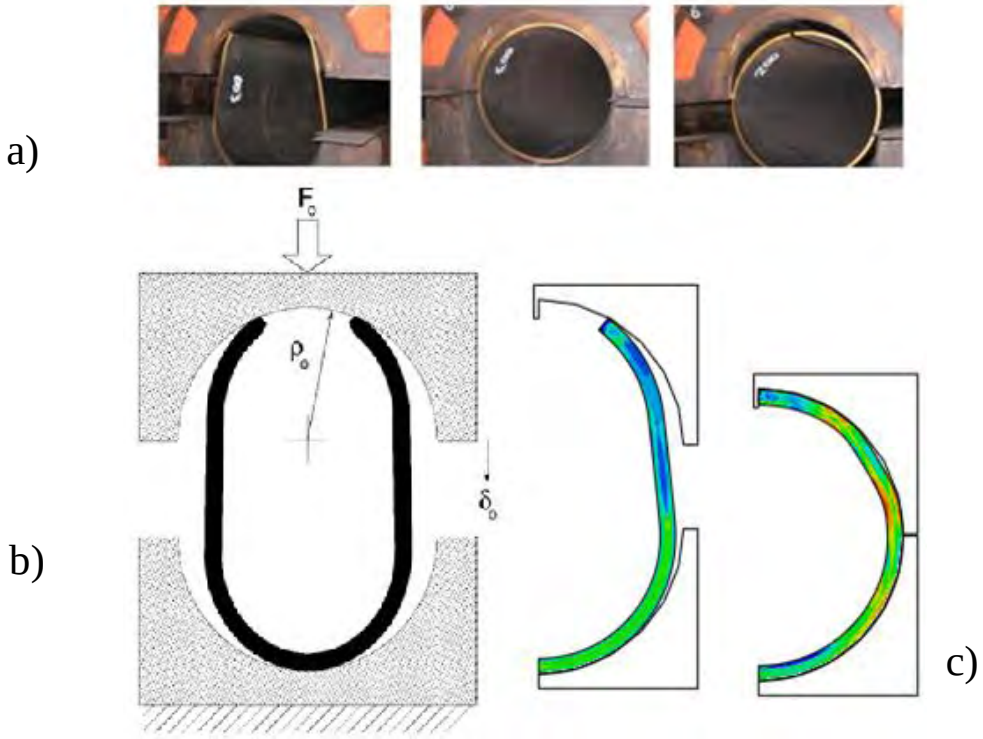

Figure 9: O-ing phase: the semi-circular die moves downwards until it touches the other die to facilitate the welding of the two beveled edges; (a) representative photos of this phase [18]; (b) Schematic representation of O-press [17] and (c) Present numerical simulation.

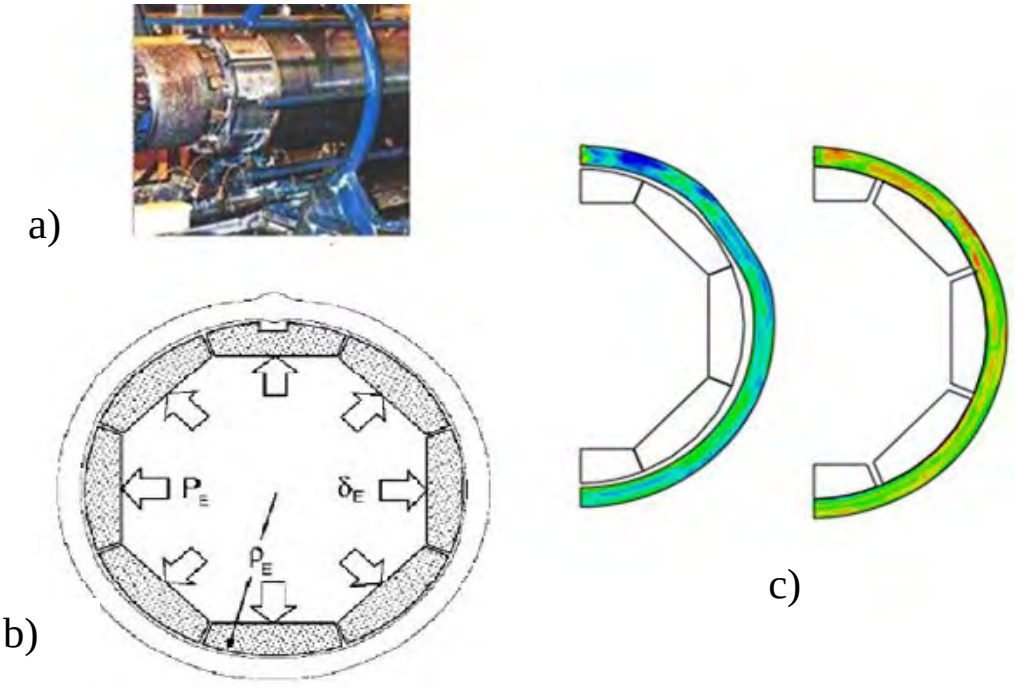

Figure 10: Expansion stage of a UOE pipe a) photo of the expansion device [17]; b) schematic representation of UOE expansion [17]; c) results from the present numerical simulation with an 8-part mandrel.

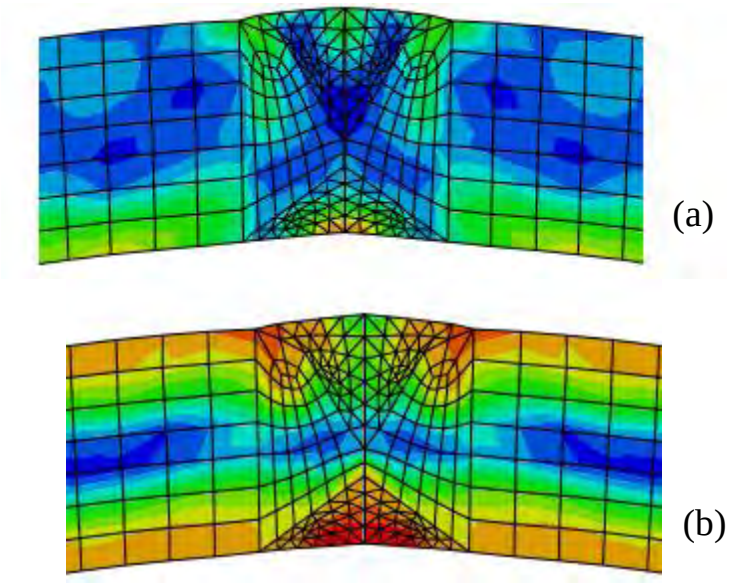

Figure 11: Present numerical simulation of the weld procedure: (a) prior the welding and (b) after the welding.

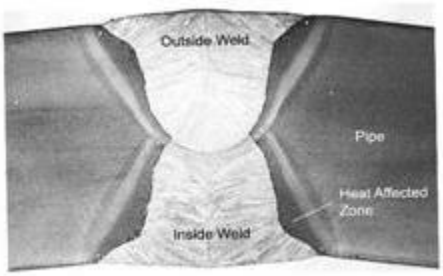

Figure 12: Welding metallography at the top edge of the plate [22].

3 Finite element modeling of the UOE process

The simulation of the UOE forming process is conducted with finite element simulation, aimed at assessing the stress (residual stresses) and strain (initial imperfections, initial ovalization) field at the end of the forming process. The numerical simulation continues with the examination of the pipe performance under external pressure and pressureand bending.

The simulation is two-dimensional under generalized plane strain conditions. This allows the application of longitudinal bending on the symmetry plane on the formed pipe. In addition, due to symmetry only half of the pipe is modeled. The simulation is realized in the ABAQUS finite element software using a user-defined nonlinear kinematic hardening plasticity subroutine. For the discretization of the main part of the plate, linear, reduced integration generalized plane-strain continuum finite elements are used (CPEG4R). The "Static, General" algorithm was used for simulating the forming process, while the "Static, Riks" algorithm was employed for simulating the external pressure application, and subsequently the application of bending in presence of external pressure.

An interesting aspect of the numerical simulation is the modeling of the forming dies. Herein, the dies are modeled as analytical rigid surfaces, as opposed to the deformable steel plate. For the interaction between the surfaces of the plate and the dies, a "master-slave" type algorithm is adopted, where the rigid surfaces of the dies are the "master" surfaces and the deformable surfaces of the steel plate are the "slave" surfaces in a contact pair. These contact pairs are allowed to slide without friction. In every step, all the "active" and "inactive" bodies are defined using the appropriate commands. This is necessary because in each step of the forming process, certain bodies are used (active bodies) while others are neglected (inactive bodies).

In order to simulate the welding procedure, an additional material in the bevel of the welding is assumed in the original geometry. In order to keep the UOE process unaffected until the end of the O phase (Figure 9), this particular part is considered with a small Young's modulus (equal to 5% of the Young's modulus assumed in the rest part of the steel plate). Immediately after the welding phase, a small step is performed where this material is replaced with a material which has the same Young's modulus with the base plate material and 6% greater yield strength from the base steel of the plate corresponding to overmatched weld. During this step the plate is restrained at its lower point. It is noted that the welding part is discretized using CPEG3 linear, three-node finite elements. The finite element mesh of UOE model at the edge of the plate is shown in Figure 13.

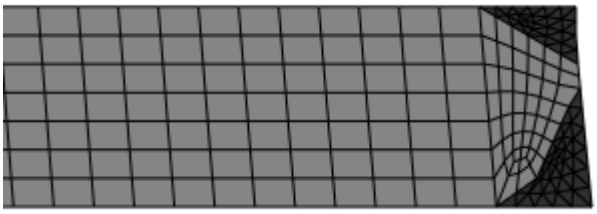

Figure 13: The finite element mesh of UOE model at the beveled edge of the plate.

4 Material behavior and modeling

A significant part of the present study is the development and implementation of an efficient constitutive model. This constitutes a key issue for the reliable prediction of the UOE manufacturing process, as well as the prediction of the structural response due to the influence of the manufacturing process.

The material behavior under reverse or cyclic loading is of major importance for the accurate simulation of the UOE process, as well as for the reliable prediction of the buckling strength under external pressure and bending capacity. The reverse loading of metal is characterized by a "rounded" stress-strain curve as shown in Figure 14, due to Bauschinger effect. The plasticity model, which is presented in this chapter is capable of describing the plastic plateau at initial yielding of the steel plate, as well as the Bauschinger effect and the rounded stress-strain curve at re-loading stages (hysteresis loop)

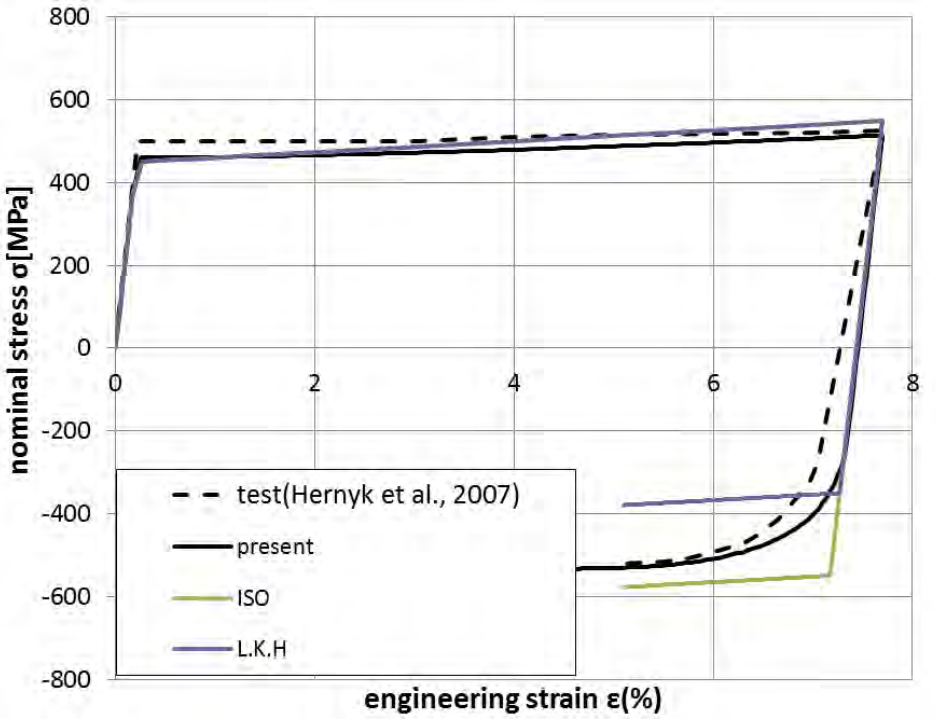

Figure 14: Material modeling, for the uniaxial stress – strain curve obtained experimentally by Herynk et al. [17].

4.1 Nonlinear kinematic/isotropic (combined) hardening model with plateau

The plasticity model under consideration, has the following feature similar to numerous classical metal plasticity models,

a) The von Mises yield criterion:

$$F(\boldsymbol{\sigma}-\boldsymbol{\alpha})=\frac{1}{2}(\mathbf{s}-\mathbf{a})\cdot(\mathbf{s}-\mathbf{a})-\frac{k^2}{3}=0 \tag{4.1}$$

where $\mathbf{s}$ is the deviatoric stress tensor defined as $\mathbf{s}=\boldsymbol{\sigma}-p\mathbf{I}$ (p is the equivalent pressure stress and $\mathbf{I}$ is the identity tensor), $\mathbf{a}$ is the back stress tensor that expresses the current center of the yield surface in the deviatoric space and k is the parameter that defines the size of the yield surface.

b) The flow rule, written here in a more general form:

$$\dot{\varepsilon}^p=\frac{1}{H}\left\langle\frac{\partial F}{\partial\boldsymbol{\sigma}}\cdot\dot{\boldsymbol{\sigma}}\right\rangle\frac{\partial F}{\partial\boldsymbol{\sigma}} \tag{4.2}$$

Where ε^p is the plastic strain tensor, H is the plastic modulus. Also, $\langle\ \rangle$ indicates the MacCauley bracket and the dot express the inner product of two tensors.

c) The kinematic hardening rule:

$$\dot{\mathbf{a}}=g(\boldsymbol{\sigma},\boldsymbol{\varepsilon}^p,\mathbf{a},\dot{\boldsymbol{\sigma}},\dot{\boldsymbol{\varepsilon}}^p,etc) \tag{4.3}$$

The kinematic hardening rule dictates the evolution of the yield surface during aplastic loading increment is by translation in the stress space only. Among other models, in this study the Armstrong and Frederick model is taken as a basic Armstrong and Frederick [20] have proposed the first nonlinear kinematic hardening rule. They introduced a kinematic hardening

rule for the “backstress” tensor, which contains a “recall” term, which represents the fading memory effect of the strain path and makes the rule nonlinear.

The kinematic hardening rule in this model is given in the form:

$$\dot{\mathbf{a}} = C(\varepsilon_{qpl})\dot{\boldsymbol{\varepsilon}}^{p} - \gamma\boldsymbol{\alpha}\dot{\varepsilon}_{q} \tag{4.4}$$

$$\dot{\varepsilon}_{q} = \sqrt{\frac{2}{3}\dot{\boldsymbol{\varepsilon}}^{P}\cdot\dot{\boldsymbol{\varepsilon}}^{P}} \tag{4.5}$$

$\dot{\varepsilon}_{q}$ is the increment of equivalent plastic strain and $C(\varepsilon_{qpl})$, γ are parameters calibrated from cyclic test data. More specifically, $C(\varepsilon_{qpl})$ is the kinematic hardening function, which is a function of equivalent plastic strain ε_{qpl} added every time a plastic region is reached, and γ determines the rate at which the kinematic hardening modulus decreases with increasing plastic deformation.

The original Armstrong – Frederick model assumes that the size of the yield surface is constant. In the present study this condition is relaxed so that the yield surface is allowed to change depending on the amount of the equivalent plastic strain:

$$k = k(\varepsilon_{q}) \tag{4.6}$$

The equation describing the von Mises yield surface is now written as:

$$F = \frac{1}{2}(\mathbf{s}-\mathbf{a})\cdot(\mathbf{s}-\mathbf{a}) - \frac{k^{2}(\varepsilon_{q})}{3} = 0 \tag{4.7}$$

where $k(\varepsilon_{q})$ is a function of the equivalent plastic strain that defines the size of the yield. Eq.(4.7) is considered as a mixed-hardening equation.

Using (4.7),the plastic strain rate equation becomes

$$\dot{\boldsymbol{\varepsilon}}^{p} = \dot{\lambda}\frac{\partial F}{\partial \boldsymbol{\sigma}} = \dot{\lambda}(\mathbf{s}-\mathbf{a}) \tag{4.8}$$

In addition the equivalent plastic strain rate becomes

$$\dot{\varepsilon}_q = \sqrt{\frac{2}{3}\dot{\boldsymbol{\varepsilon}}^{P}\cdot\dot{\boldsymbol{\varepsilon}}^{P}} \tag{4.9}$$

with the aid of (4.8) one obtains

$$\dot{\varepsilon}_q = \frac{2}{3}\dot{\lambda}k(\varepsilon_q) \tag{4.10}$$

or equivalently

$$\dot{\lambda} = \frac{3}{2}\frac{\dot{\varepsilon}_q}{k(\varepsilon_q)} \tag{4.11}$$

Combining the above equations,

$$\dot{\boldsymbol{\varepsilon}}^{p} = \frac{3}{2k(\varepsilon_q)}\dot{\varepsilon}_q(\mathbf{s}-\mathbf{a}) \tag{4.12}$$

Enforcing the consistency condition $\dot{F}=0$ the following equation is obtained:

$$\frac{\partial F}{\partial \boldsymbol{\sigma}}\cdot\dot{\boldsymbol{\sigma}} + \frac{\partial F}{\partial \mathbf{a}}\cdot\dot{\mathbf{a}} + \frac{\partial F}{\partial k}\cdot\dot{k} = 0 \tag{4.13}$$

where

$$\dot{k} = \frac{dk(\varepsilon_q)}{d\varepsilon_q}\dot{\varepsilon}_q \tag{4.14}$$

From equations (4.4),(4.7), (4.13), (4.14) $\dot{\varepsilon}_q$ can be computed as follows

$$\dot{\varepsilon}_q = \frac{1}{\left[kC(\varepsilon_{qpl}) - \gamma\mathbf{a}\cdot(\mathbf{s}-\mathbf{a}) + \frac{2}{3}k(\varepsilon_q)\frac{dk(\varepsilon_q)}{d\varepsilon_q}\right]}(\mathbf{s}-\mathbf{a})\cdot\dot{\mathbf{s}} \tag{4.15}$$

Substitution of Eq. (4.15) into Eq.(4.12), results in the following expression for the plastic strain rate:

$$\dot{\boldsymbol{\varepsilon}}^{\mathbf{p}} = \frac{3}{2k}\frac{1}{\left[kC(\varepsilon_{qpl}) - \gamma\mathbf{a}\cdot(\mathbf{s}-\mathbf{a}) + \frac{2}{3}k(\varepsilon_q)\frac{dk(\varepsilon_q)}{d\varepsilon_q}\right]}[(\mathbf{s}-\mathbf{a})\cdot\dot{\mathbf{s}}](\mathbf{s}-\mathbf{a}) \tag{4.16}$$

In addition, it is necessary to evaluate $\mathbf{D}^{ep}$ which is the fourth-order elastoplastic rigidity tensor. In order to evaluate $\mathbf{D}^{ep}$ the elasticity equation used is

$$\boldsymbol{\sigma} = \mathbf{D}\boldsymbol{\varepsilon}^{e} \tag{4.17}$$

where $\mathbf{D}$ is the fourth-order elastic rigidity tensor and $\boldsymbol{\varepsilon}^{e}$ is the elastic strain tensor. Equation (4.17) can also be written in its rate form

$$\dot{\boldsymbol{\sigma}} = \mathbf{D}\dot{\boldsymbol{\varepsilon}}^{e} \tag{4.18}$$

assuming that the total strain tensor is decomposed into an elastic and a plastic part:

$$\boldsymbol{\varepsilon} = \boldsymbol{\varepsilon}^{e} + \boldsymbol{\varepsilon}^{p} \tag{4.19}$$

Using the above substituting in to the rate form of the general elasticity equation one obtains:

$$\dot{\boldsymbol{\sigma}} = \mathbf{D}(\dot{\boldsymbol{\varepsilon}} - \dot{\boldsymbol{\varepsilon}}^{P}) \tag{4.20}$$

or equivalently

$$\dot{\boldsymbol{\sigma}} = \mathbf{D}\dot{\boldsymbol{\varepsilon}} - \mathbf{D}\dot{\lambda}(\mathbf{s} - \mathbf{a}) \tag{4.21}$$

Since $(\mathbf{s} - \boldsymbol{\alpha})$ is a deviatoric tensor, one can readily show that the product $\mathbf{D}(\mathbf{s} - \boldsymbol{\alpha})$ is equal to $2G(\mathbf{s} - \boldsymbol{\alpha})$. Using this tensor property and Eq.(4.11), Eq.(4.21) can be rewritten as:

$$\dot{\boldsymbol{\sigma}} = \mathbf{D}\dot{\boldsymbol{\varepsilon}} - \frac{3G}{k}\dot{\varepsilon}_{q}(\mathbf{s} - \mathbf{a}) \tag{4.22}$$

For the simplification of the product $[(\mathbf{s} - \mathbf{a}) \cdot \dot{\mathbf{s}}]$ in Eq.(4.15), both parts of the rate form of the general elasticity equation are multiplied with the term $(\mathbf{s} - \mathbf{a})$.

This results in:

$$\dot{\mathbf{s}} \cdot (\mathbf{s} - \mathbf{a}) = (\mathbf{D}\dot{\boldsymbol{\varepsilon}}) \cdot (\mathbf{s} - \mathbf{a}) - \frac{3G}{k}\dot{\varepsilon}_{q}(\mathbf{s} - \mathbf{a}) \cdot (\mathbf{s} - \mathbf{a}) \tag{4.23}$$

or equivalently

$$\dot{\mathbf{s}} \cdot (\mathbf{s} - \mathbf{a}) = (\mathbf{D}\dot{\boldsymbol{\varepsilon}}) \cdot (\mathbf{s} - \mathbf{a}) - 2Gk\dot{\varepsilon}_{q} \tag{4.24}$$

and using Eq.(4.15) the final expression of the equivalent plastic strain rate is

$$\dot{\varepsilon}_q = \frac{1}{B}\left(\mathbf{D}\dot{\boldsymbol{\varepsilon}}\right)\cdot(\mathbf{s}-\mathbf{a}) \tag{4.25}$$

where

$$\mathrm{B} = kC(\varepsilon_{qpl}) - \gamma\mathbf{a}\cdot(\mathbf{s}-\mathbf{a}) + \frac{2}{3}k(\varepsilon_q)\frac{dk(\varepsilon_q)}{d\varepsilon_q} + 2Gk \tag{4.26}$$

Defining tensor $\boldsymbol{\xi}$ as the tensor difference $\mathbf{s}-\mathbf{a}$ and using Eq.(4.25), Eq.(4.26) for the incremental stress-strain relations can be rewritten as:

$$\dot{\boldsymbol{\sigma}} = \left(\mathbf{D} - \frac{6G^2}{kB}(\boldsymbol{\xi}\otimes\boldsymbol{\xi})\right)\dot{\boldsymbol{\varepsilon}} \tag{4.27}$$

where

$$\mathbf{D}^{ep} = \mathbf{D} - \frac{6G^2}{kB}(\boldsymbol{\xi}\otimes\boldsymbol{\xi}) \tag{4.28}$$

In the above expresions $\mathbf{D}^{ep}$ is the fourth-order elastoplastic rigidity tensor and $\otimes$ denotes the, forth-order tensor product of two second order tensors.

One of the drawbacks of the classical Armstrong-Frederick model is its inability to describe the abrupt change of the stress-strain curve after the initial yielding. In addition, it cannot describe the yield plateau regions. However, most structural steels exhibit a plastic plateau region after the initial material yielding. This region, also known as "Luders region", is extended up to a certain strain level usually 1.5-2% before the material enters the strain hardening region. With reverse plastic loading, the plastic plateau disappears. Due to its inability to describe Luders plateau, modification of the aforementioned plasticity model is necessary in order to account for this features in a phenomenological manner.

In the present study, a modified Armstrong-Frederick model is adopted, initially proposed by Ucak and Tsopelas [21], where a critical plastic strain ε_{qcr} is defined as the point, at which plastic plateau region ends. Within the plateau, the equivalent plastic strain is less than the

value of ε_{qcr}, a very small constant value of C is assumed and γ is equal to zero. Outside the plateau C and γ take the original form as shown in Eq (4.4)

In a multi-axial stress state if unloading from the plateau occurs an angle-change criterion is necessary to differentiate between plastic reloading or reverse plastic loading. This depends on the orbit of the stress as shown in Figure 15. In such a case, having recording the last plastic loading vector $\boldsymbol{v}_{old}$ in the plateau, the angle between that vector and the new plastic loading direction vector $\boldsymbol{v}_{new}$ is computed. When this angle is less than 90 degrees (θ_1 as shown in Figure 15) then the plastic plateau feature is activated. On the other hand, if the angle change is more than 90 degrees (θ_2) the standard form the nonlinear kinematic hardening is considered.

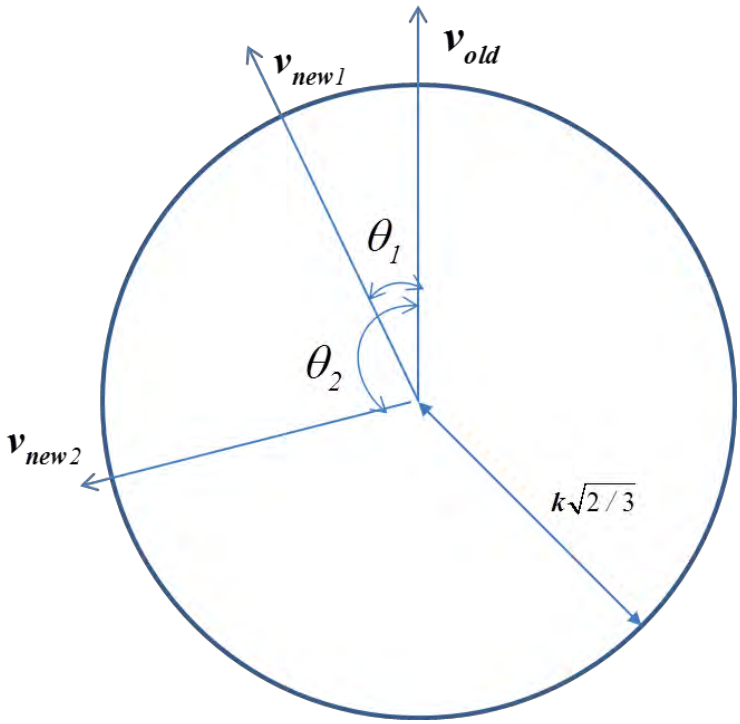

Figure 15: Schematic view of angle-change criterion .

4.2 Numerical implementation of the nonlinear kinematic/isotropic (combined) hardening model.

The numerical implementation of the nonlinear kinematic /isotropic hardening model follows an "elastic predictor – plastic corrector" scheme. The problem can be stated as follows: for given state $(\mathbf{s}_n, \mathbf{a}_n, \varepsilon_{qn})$ and a given strain increment $\Delta\boldsymbol{\varepsilon}$, calculate the new state parameters $(\mathbf{s}_{n+1}, \mathbf{a}_{n+1}, \varepsilon_{qn+1})$. More specifically the steps are described as follows

1. Elastic Prediction

Following a simple integration of the elasticity equations, elastic prediction stress $\boldsymbol{\sigma}^{(e)}$ can be written as:

$$\boldsymbol{\sigma}^{(e)} = \boldsymbol{\sigma}_n + \mathbf{D}\Delta\boldsymbol{\varepsilon} \tag{4.29}$$

The deviatoric form of the above equation is

$$\mathbf{s}^{(e)} = \mathbf{s}_n + \mathbf{D}\Delta\boldsymbol{\varepsilon} \tag{4.30}$$

Since no plastic loading is assumed to take place during this step:

$$\begin{aligned} \Delta\mathbf{a} &= 0 \\ \Delta\varepsilon_q &= 0 \end{aligned} \tag{4.31}$$

A check must be performed to examine whether the yield criterion is satisfied:

$$F = \frac{1}{2}(\mathbf{s}^{(e)} - \mathbf{a}_n)\cdot(\mathbf{s}^{(e)} - \mathbf{a}_n) - \frac{k^2(\varepsilon_{qn})}{3} \le 0 \tag{4.32}$$

If satisfied, then elastic stress prediction is valid and the step is elastic. In such a case

$$\mathbf{a}_{n+1} = \mathbf{a}_n \tag{4.33}$$

$$\boldsymbol{\sigma}_{n+1} = \boldsymbol{\sigma}^{(e)} \tag{4.34}$$

$$\mathbf{s}_{n+1} = \mathbf{s}^{(e)} \tag{4.35}$$

$$\varepsilon_{qn+1} = \varepsilon_{qn} \tag{4.36}$$

$$\varepsilon_{qpln+1} = \varepsilon_{qpln} = 0 \tag{4.37}$$

If it is not satisfied, then one should proceed to the Plastic Corrector step.

2. Plastic Corrector Step

The nonlinear kinematic hardening rule:

$$\dot{\mathbf{a}} = C(\varepsilon_{qpl})\dot{\boldsymbol{\varepsilon}}^p - \gamma \mathbf{a}\dot{\varepsilon}_q \tag{4.38}$$

can be written

$$\dot{\mathbf{a}} = C(\varepsilon_{qpl})\frac{3}{2k}\dot{\varepsilon}_q(\mathbf{s}-\mathbf{a}) - \gamma \mathbf{a}\dot{\varepsilon}_q \tag{4.39}$$

Substituting $\boldsymbol{\xi}$ for $(\mathbf{s}-\mathbf{a})$ and integrating over the step using an Euler-backward scheme one results in:

$$\mathbf{a}_{n+1} = \mathbf{a}_n + C(\varepsilon_{qp\ln+1})\frac{3}{2k(\varepsilon_{qn+1})}\Delta\varepsilon_q\boldsymbol{\xi}_{n+1} - \gamma\mathbf{a}_{n+1}\Delta\varepsilon_q \tag{4.40}$$

Equivalently,

$$\mathbf{a}_{n+1} = \frac{1}{1+\gamma\Delta\varepsilon_q}\left(\mathbf{a}_n + C(\varepsilon_{qp\ln+1})\frac{3}{2k(\varepsilon_{qn+1})}\Delta\varepsilon_q\boldsymbol{\xi}_{n+1}\right) \tag{4.41}$$

Integrating the elasticity equations:

$$\Delta\boldsymbol{\sigma} = \mathbf{D}\Delta\boldsymbol{\varepsilon} - \mathbf{D}\Delta\boldsymbol{\varepsilon}^p \tag{4.42}$$

The above equation is written as:

$$\begin{aligned}\boldsymbol{\sigma}_{n+1} &= \boldsymbol{\sigma}_n + \mathbf{D}\Delta\boldsymbol{\varepsilon} - \mathbf{D}\Delta\boldsymbol{\varepsilon}^p \\ \boldsymbol{\sigma}_{n+1} &= \boldsymbol{\sigma}^{(e)} - 2G\Delta\boldsymbol{\varepsilon}^p\end{aligned} \tag{4.43}$$

Furthermore, using Euler-backward integration scheme, the flow rule is integrated as follows:

$$\Delta\boldsymbol{\varepsilon}^p = \frac{3}{2k(\varepsilon_{qn+1})}\Delta\varepsilon_q(\mathbf{s}_{n+1} - \mathbf{a}_{n+1}) \tag{4.44}$$

and using the deviatoric tensor property of the rigidity tensor:

$$\mathbf{D}(\mathbf{s}-\boldsymbol{\alpha}) = 2G\boldsymbol{\xi} \tag{4.45}$$

The deviatoric part of the above equation is written as:

$$\mathbf{s}_{n+1} = \mathbf{s}^{(e)} - \frac{3G}{k(\varepsilon_{qn+1})}\Delta\varepsilon_q\boldsymbol{\xi}_{n+1} \tag{4.46}$$

the tensor $\boldsymbol{\xi}_{n+1}$ can be written as follows:

$$\boldsymbol{\xi}_{n+1} = \mathbf{s}^{(e)} - \frac{3G}{k(\varepsilon_{qn+1})}\Delta\varepsilon_q\boldsymbol{\xi}_{n+1} - \frac{1}{1+\gamma\Delta\varepsilon_q}\left(\mathbf{a}_n + C(\varepsilon_{qp\ln+1})\frac{3}{2k(\varepsilon_{qn+1})}\Delta\varepsilon_q\boldsymbol{\xi}_{n+1}\right) \tag{4.47}$$

Equivalently:

$$\boldsymbol{\xi}_{n+1} = \frac{1}{AFACT}\left(\mathbf{s}^{(e)} - \frac{1}{1+\gamma\Delta\varepsilon_q}\mathbf{a}_n\right) \tag{4.48}$$

Where

$$AFACT = 1 + \frac{3}{k(\varepsilon_{qn+1})}\left(G + \frac{C(\varepsilon_{qp\ln+1})}{2(1+\gamma\Delta\varepsilon_q)}\right)\Delta\varepsilon_q \tag{4.49}$$

Because of the consistency property of the flow rule, the new state parameters should satisfy the yield condition. This equation results in a nonlinear algebraic equation in terms of $\Delta\varepsilon_q$.

$$\frac{1}{2}\boldsymbol{\xi}_{n+1}\cdot\boldsymbol{\xi}_{n+1} - \frac{1}{3}k^2(\varepsilon_{qn+1}) = 0 \tag{4.50}$$

The above equation is solved in terms of the unknown $\Delta\varepsilon_q$ with the use of an iterative Newton – Raphson scheme as follows:

$$\Delta\varepsilon_{q(i+1)} = \Delta\varepsilon_{q(i)} - \frac{f\left(\Delta\varepsilon_q\right)_{(i)}}{f'\left(\Delta\varepsilon_q\right)_{(i)}} \tag{4.51}$$

where

$$f'\left(\Delta\varepsilon_q\right)=\frac{df\left(\Delta\varepsilon_q\right)}{d\Delta\varepsilon_q}$$

The nonlinear procedure is continued until the following criterion is satisfied:

$$\frac{\Delta\varepsilon_{q(i+1)}}{\Delta\varepsilon_{q(i)}}\le e_{Tol}$$

where e_{Tol} is the desired tolerance.

The new equivalent plastic strain is equal to

$$\varepsilon_{qn+1}=\varepsilon_{qn}+\Delta\varepsilon_q \tag{4.52}$$

and

$$\varepsilon_{qpln+1}=\varepsilon_{qpln}+\Delta\varepsilon_q \tag{4.53}$$

If the ε_{qn+1} is less than the critical value ε_{qcr}, the angle change is performed. More specifically

$\mathbf{v}_{old}$, $\mathbf{v}_{new}$ are the plastic loading vector calculated as:

$$\mathbf{v}_{old}=\frac{\mathbf{s}_n-\mathbf{a}_n}{\left|\mathbf{s}_n-\mathbf{a}_n\right|},\ \mathbf{v}_{new}=\frac{\mathbf{s}_{n+1}-\mathbf{a}_{n+1}}{\left|\mathbf{s}_{n+1}-\mathbf{a}_{n+1}\right|} \tag{4.54}$$

The angle between $\mathbf{v}_{old}$, $\mathbf{v}_{new}$ is defined using the inner product rule:

$$\theta=\cos^{-1}(\mathbf{v}_{old}\cdot\mathbf{v}_{new}) \tag{4.55}$$

If θ is less than 90 degrees the function of $C(\varepsilon_{qpl})$ is constant and equal with a small value in any other case $C(\varepsilon_{qpl})$ is function of ε_{qpl}

If ε_{qn+1} is more than the critical ε_{qcr}, $C(\varepsilon_{qpl})$ is function of ε_{qpl}. Moreover, it is important to note that after yielding, the first value of the hardening modulus is the hardening used for the plateau region which is quite small compared to the hardening for the Bauschinger effect.

Function $k(\varepsilon_q)$ can be considered in several forms. Herein it is considered based on experimental data, in order to take into account material behavior, according to the following equation:

$$k(\varepsilon_q) = \sigma_{yield} + Q(1 - e^{-b\varepsilon_q}) \tag{4.56}$$

where Q, b are isotropic hardening parameters. More specifically, Q is the maximum expected change of the yield surface size, which may have positive or negative values referring to material hardening or softening respectively, and b is an exponent, representing the rate at which the change takes place. Moreover, in the classical Amstrong Frederic model C is constant where the present model uses a function $C(\varepsilon_{qpl})$ in order to describe more efficiently Bauschinger effect under reverse plastic loading. The equation used has the following form:

$$C(\varepsilon_{qpl}) = C_0 + Q_b(1 - e^{-c\varepsilon_{q\,pl}}) \tag{4.57}$$

where Q_b is the maximum expected change of the initial hardening modulus, which may take negative values, and c is an exponent representing the rate at which this change takes place.

4.3 Verification of UMAT

For the verification of the present constitutive model, cyclic-loading material tests, performed at the University of Porto (FEUP) [25] have been simulated using finite element software ABAQUS and the developed UMAT subroutine. The steel grade is X52 and the geometry of the specimen and the finite element mesh is presented in (Figure16 and Figure 17). The result of the simulation is illustrated in Figure 18. The figure demonstrates that the model is capable at describing both the plateau region and the Baushinger effect.

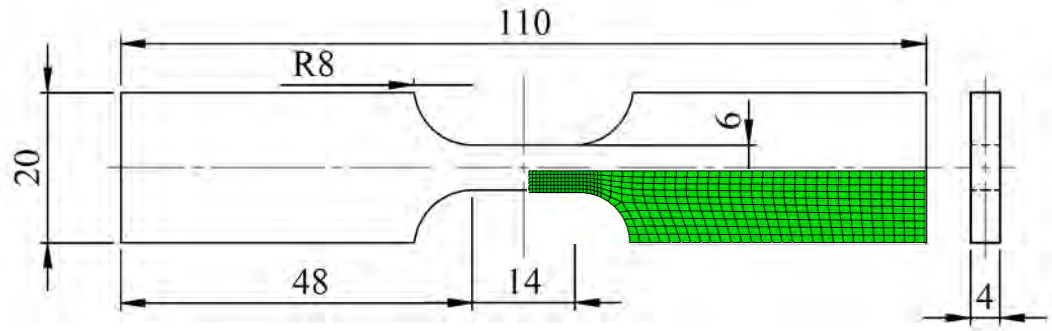

Figure16:Specimen geometry – FEUP (2013) [25].

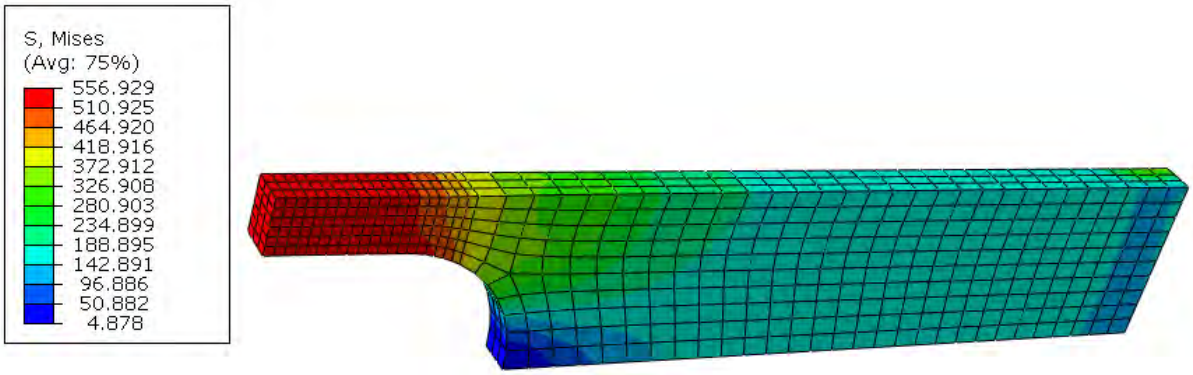

Figure 17: The numerical model for simulating FEUP cyclic tests.

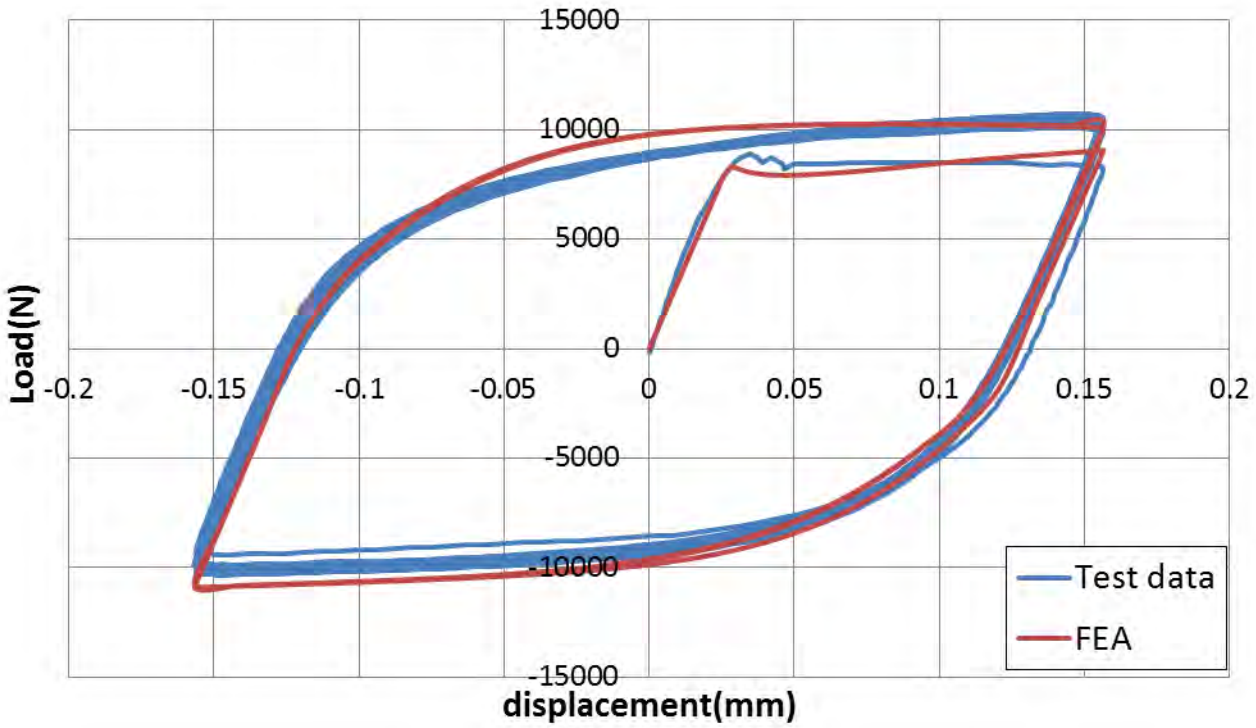

Figure 18: Experimental and numerical load-displacement curves.

5 Numerical results of UOE process

5.1 Description of case study

The developed numerical model described in the previous paragraph is utilized to study a pipe of 609.6 mm external nominal diameter (24 in) and 32.3 mm wall thickness (1.273 in). A similar case study is considered by Herynk et al [17]. The material of the steel plate material is assumed to have Young modulus E=210GPa, yield stress σ_y =460MPa (65ksi) and Poisson ratio ν=0.3 (X65 steel grade). The plasticity model adopted for this analysis is described in the previous chapter. The model has been calibrated based on a uniaxial stress-strain response as shown in Figure 14. The material curve used for the calibration of the numerical model is obtained from Herynk*et al.*[17]. The test in Figure 14 has indicated a decrease of Young's modulus during unloading. However, this feature is not taken into account in the present study. All the forming parameters and the plate characteristics used in the present analysis are reported in Table 1, which are similar to the parameters considered in [17].

Table1: Characteristics of the UOE numerical simulation [17].

	Symbol	Description	Value
Plate	t	Plate thickness (mm)	32.33
	W	Plate width (mm)	1803
	σ_y	Steel yield stress (MPa)	460
Crimping	ρ_{CRi}	Internal crimping radius (mm)	265.4
	ρ_{CRo}	External crimping radius (mm)	298.5
	δ_{CR}	Final distance of the 2 dies (mm)	0.5
	L_{CR}	Horizontal distance of the dies (mm)	676.7
	h_{CR}	Height of the external crimping die (mm)	150
U-ing	ρ_U	U-Punch radius (mm)	246.4
	δ_U	Distance covered by the U-Punch (mm)	724
	δ_r	Distance covered by the Roller (mm)	102
	h_r	Horizontal Roller position (mm)	457
	υ_r	Vertical position of the Anvil (mm)	724
O-ing	ρ_O	Radius of the semi-circular dies (mm)	303.8
	δ_O	Overlap of the O-dies' centers (mm)	0
Expansion	ρ_E	Mandrel radius (mm)	260
	δ_E	Expansion value (mm)	7.75
	N_E	Mandrel segments	8

5.2 Numerical results

In the present study a parametric analysis of the effect of expansion is taken into consideration. In the numerical simulation, the Expansion takes place in two stages. During the initial stage, the mandrels move outwards (radially) until all mandrels contact the pipe. This distance is denoted as δ_0 and up to that distance, bending deformation of the pipe occurs

primarily. The Expansion phase is completed with the application of an additional displacement u_E of the mandrels on the same direction. At that stage, significant axial strain is induced in the hoop direction of the pipe. The basic parameter examined herein is the additional expansion value u_E at the final stage of the forming process. Different expansion values are examined ranging from u_E =0 mm to u_E =7.75mm beyond which severe plastic deformations of the pipe take place. According to the above, the following expression can be written for the total mandrel displacement u_{Tot} :

$$u_{Tot} = \delta_0 + u_{Expansion} \tag{5.1}$$

Moreover, the ovalization parameter of the pipe cross-section Δ_0 measured at the end of the E-phase, right after pipe unloading: these two diameters are different since the pipe is not in perfect cyclic shape. Therefore, the ovalization parameter Δ_0 is a measure of geometric initial imperfection.Furthermore, the expansion stage of the UOE process induces hoop strain ε_{E} on the pipe body, which is defined in Eq.(5.2)

$$\varepsilon_{\mathrm{E}} = \frac{C_E - C_O}{C_O} \tag{5.2}$$

where C_E and C_O are mid surface circumference lengths after the Expansion and the O-ing phase, respectively. The value of C_E is measured after the mandrels are removed, and may be considered as “permanent” hoop strain, accounting for the small “elastic rebound”. Moreover, it should be underlined that the value of ε_{E} expresses an average circumferential strain due to the expansion of the pipe from the stage where all mandrels are in contact with its inner surface, until the final stage. Therefore, the ε_{E} value may not be equal to the real

strain in the pipe wall . In Figure 19 the relation between the u_E value and the corresponding permanent induced strain is depicted.

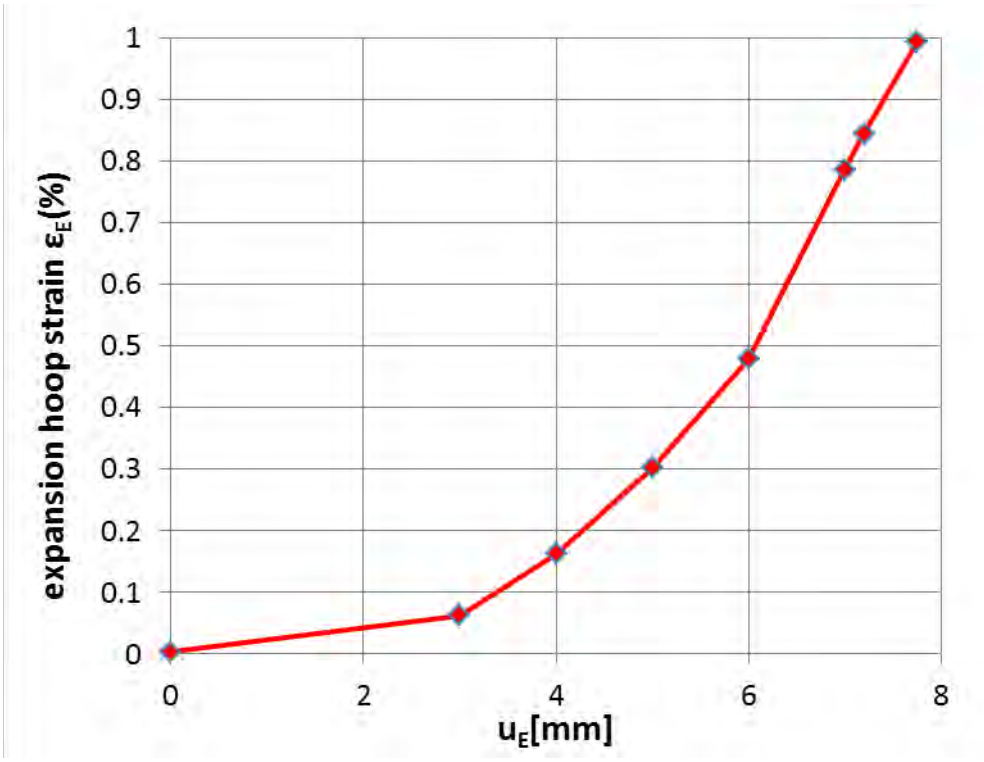

Figure 19: Variation of the expansion displacement value u_E in terms of the induced (permanent) hoop expansion strain ε_E of the formed pipe.

The mean (average) thickness of the pipe t_{ave} around the cross-section is reported in Figure 20. The results in Figure 20 show that the mean thickness of the pipe decreases significantly with increasing values of expansion hoop strain. To quantify variations of thickness around the pipe cross-section, a non-dimensional imperfection parameter is introduced, which expresses the variation of the circumferential pipe- wall thickness:

$$\Delta T = \frac{t_{\max} - t_{\min}}{t_{ave}} \tag{5.3}$$

where t_{max} is the maximum value noticed around the circumference and t_{min} is the minimum value. Note that the maximum value of thickness considered the entire circumference of the cross-section, except for the area exactly at the weld, where the weld cap may increase significantly the thickness locally.

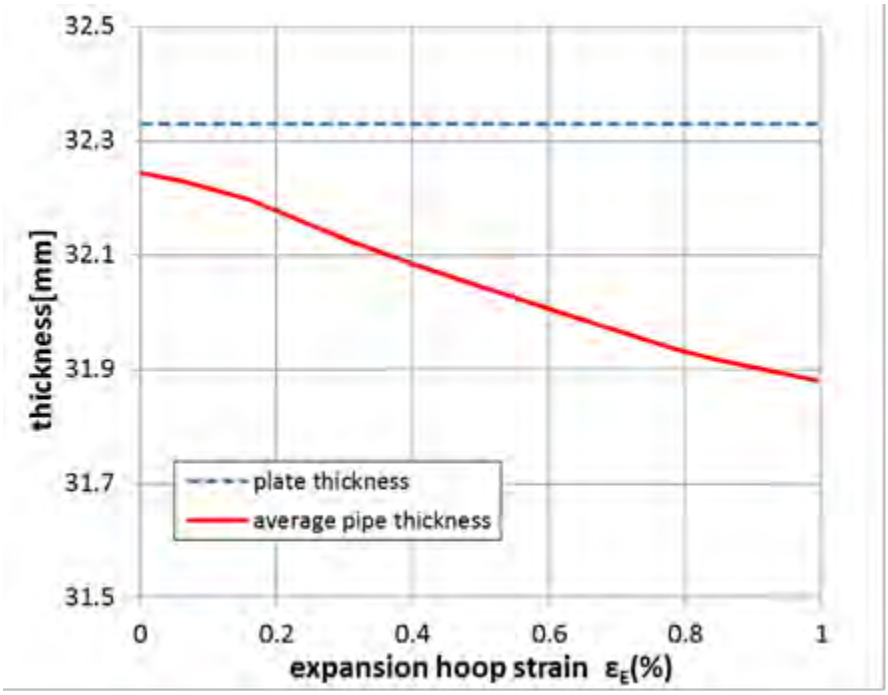

Figure 20: Effect of expansion strain ε_E to the average thickness of the UOE pipe.

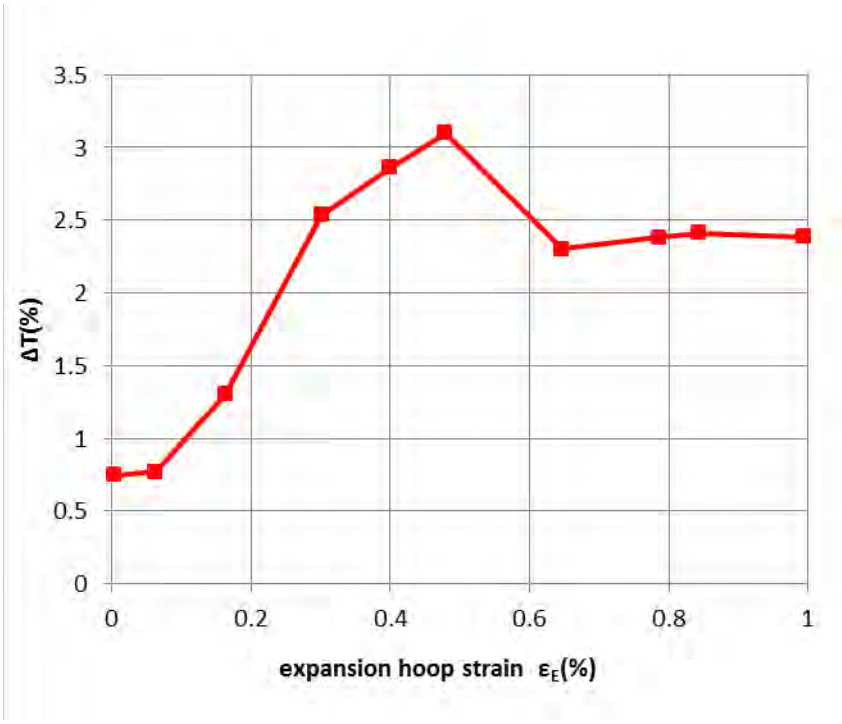

Figure 21: Effect of expansion strain on thickness imperfection of the formed pipe.

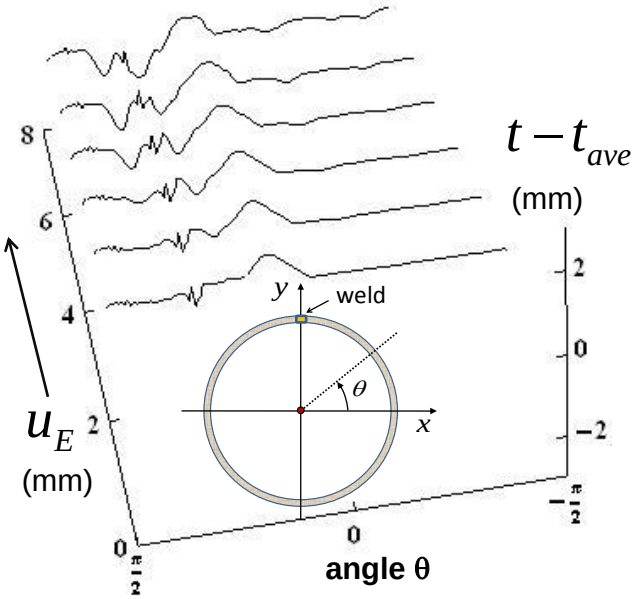

Figure 22: Effect of expansion displacement u_E on thickness variation around the circumference of the formed pipe.

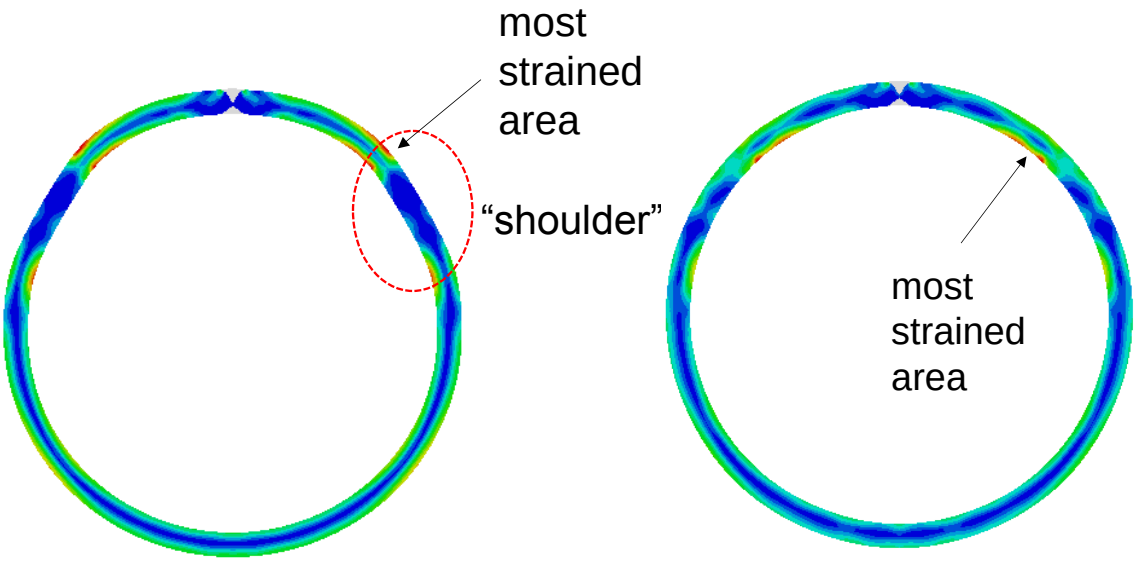

Figure 23: Final distribution of equivalent plastic strain at the final stage: (left) UO case $\varepsilon_{\mathrm{E}}=0\%$; (right) UOE case with $\varepsilon_{\mathrm{E}}=1\%$.

Figure 21 shows that there is a significant change in the value of the thickness parameter $\Delta\mathrm{T}$ for different values of ε_{E}. The variation of thickness is also shown in Figure 22. It is important to note that the deviation from the average thickness is more pronounced in the area at about 30º from the weld. In that area, after the O-phase a “shoulder” appears that is mainly responsible for the non-circularity of the pipe, as shown in Figure 23 (left). The “shoulder” disappears when expansion is performed, but this is associated with a significant plastic deformation at this location as shown in Figure 23 (right). At a certain stage of expansion, this concentration of plastic deformation results in local reduction of pipe wall thickness. Finally, Figure 22 shows that the change of thickness from $\theta=0$ to $\theta=-\pi/2$ lower part of the cross section is mainly constant. This can be attributed to the fact that both “shoulder” and the accumulation of plastic strain is mainly in the upper part of the pipe during the manufacturing process.

Another important parameter associated with the mechanical behavior of offshore pipes, which is affected significantly by the UOE process is the residual ovalization of the pipe cross – section. This may have a significant effect on structural response especially under high

external pressure. The effect of ε_E on ovality is illustrated in Figure 24. As expansion increases, the ovality drops rapidly for expansion strains up to about 0.2%. Further increase of the applied expansion strain causes only additional slight ovalization decrease. In the same figure, the numerical results, obtained using the developed material model, are presented along with the results presented by Herynk et al. [17] and the results using the more conventional values of isotropic and linear kinematic hardening reported by Varelis et al. [19]. Furthermore, the expansion improves the roundness of the pipe giving its final size and shape. Figure 23 illustrates the shape of the pipe with zero expansion (left) which has a significant deviation from the circularity because of the formation of the two "shoulders" and with the highest expansion (right) the deviation decreases. The results illustrated in Figure 25 show that small expansion values are associated with significant deviation from the circularity, as expansion increases the deviation decreases.

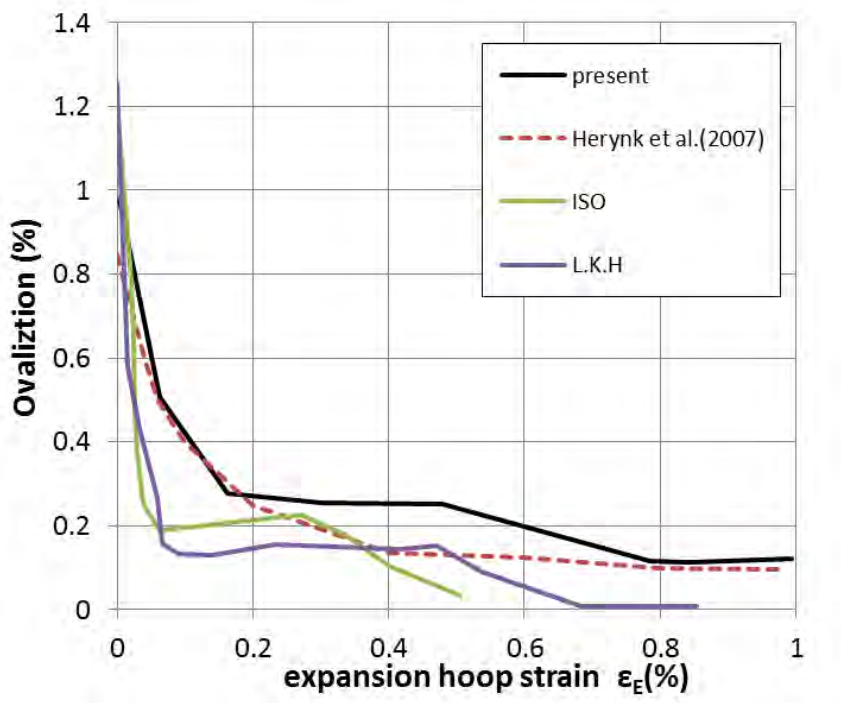

Figure 24: Ovalization parameter versus permanent strain curve for different material models.

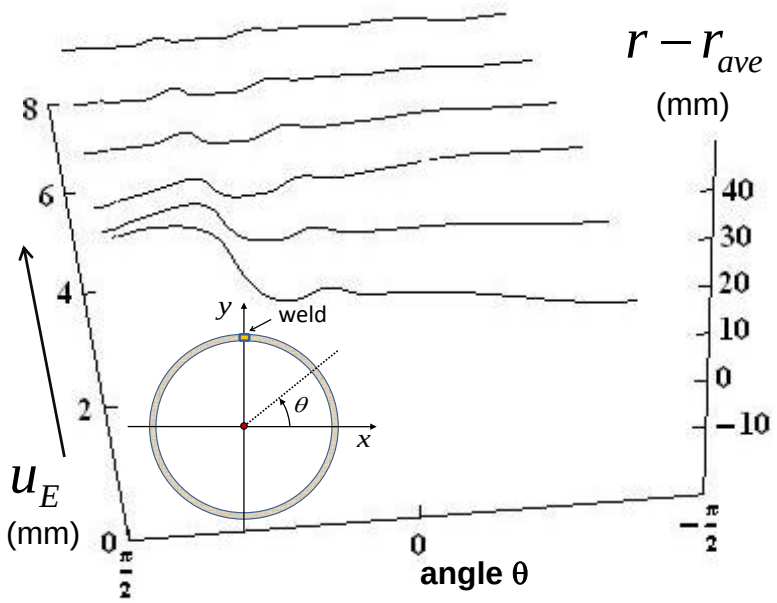

Figure 25: Effect of expansion displacement u_E on the roundness of pipe cross section.

6 Mechanical behavior during the UOE process

During the forming process the material experiences deformations far into the plastic range. The magnitude of plastic deformations induces residual stresses, which are important for the collapse pressure resistance of the pipe and the Bauschinger effect becomes more important. In the following paragraphs, the UOE process resulting stress – strain paths are presented at different locations of the pipe cross-section and the plastic deformations for each forming step are depicted. The "check points" considered in the present analysis are shown in Figure 26. At each check point both the internal and external edge of the pipe wall are examined.

During the first Crimping phase of the UOE process, all plastic deformation is located near the weld (C.P.1). The material undergoes plastic deformations until the desired curvature of the edge of the plate is achieved. The remaining part of the plate remains at low stress level (Figure 27).

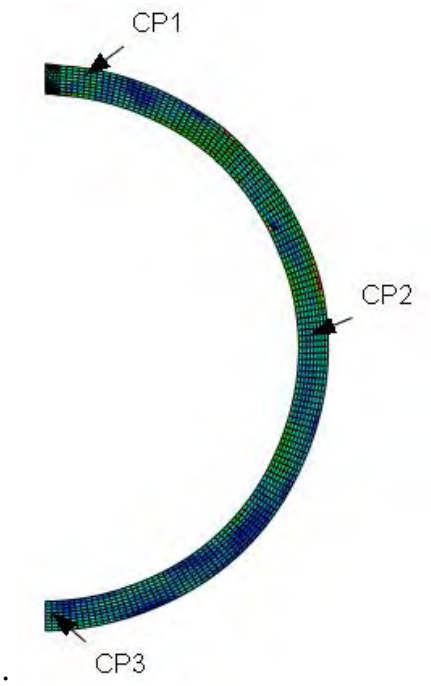

Figure 26: Location of the Check Points on the half pipe section.

In the U-ing phase that follows, stresses the areas located near points C.P.2 and C.P.3. The U-ing phase is completed with the horizontal movement of the rollers. This step “actuates” the areas near C.P.2, while the areas near C.P.1 remain mainly unaffected (Figure 28).

The O-ing phase starting afterwards results in the major change of the plate shape as shown in Figure 29. The final phase of the UOE process is the Expansion phase (Figure 30). Up to this stage, the most stressed areas of the pipe are near C.P.1 and C.P.3. Due to the expansion, all the compressive stresses that appear in the inner surface of the pipe wall throughout the forming history are relieved, while in the exterior surface of the pipe, which is in tension, tensile stresses are increased. Depending on the u_E value, the influence of this phase on the residual stress field of the pipe (i.e the final stresses at the end of the UOE process) can be an important parameter for the pipe resistance against external pressure.

Figure 31 and Figure 32 illustrate the stress – strain path in hoop direction at “check points” C.P.2, C.P.3 for u_E equal to zero expansion. It is interesting to note that the points under consideration exhibit significant plastic deformation in compression and tension respectively.

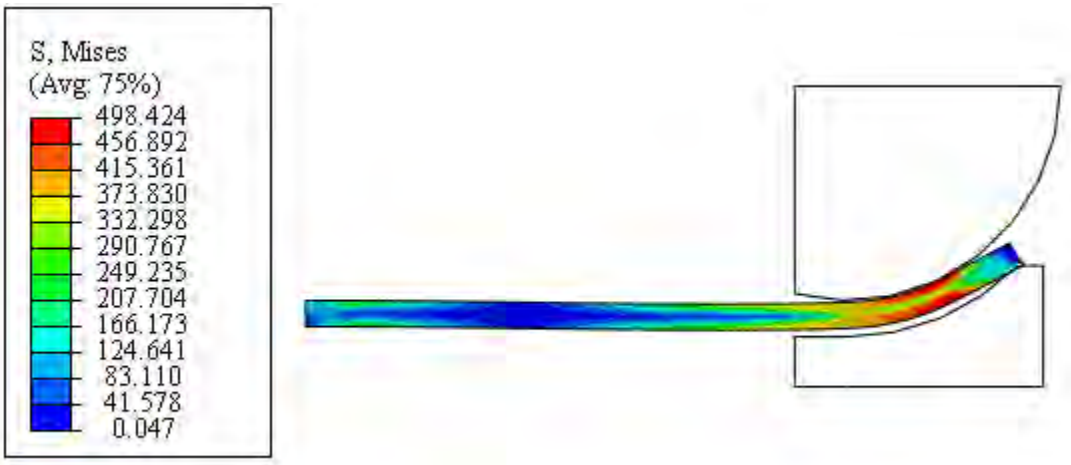

Figure 27: The numerical simulation of the UOE process ;Crimping phase.

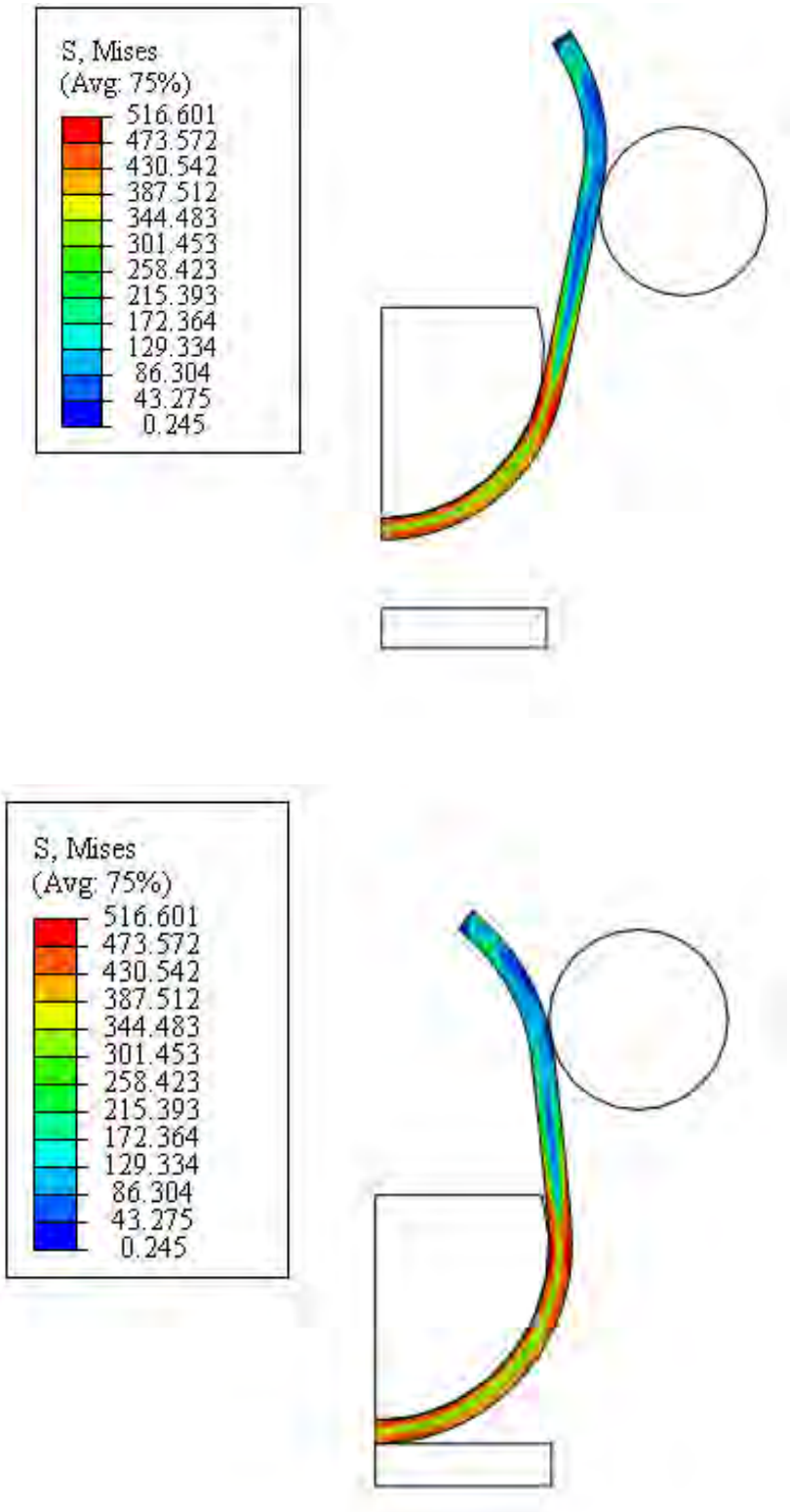

Figure 28: Numerical simulation of the UOE process ; U-ing phase.

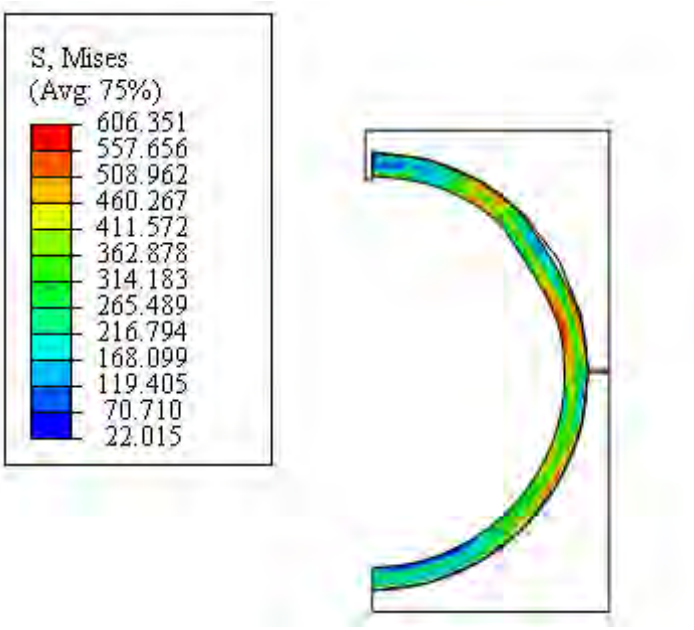

Figure 29: Numerical simulation of the UOE process ; O-ing phase.

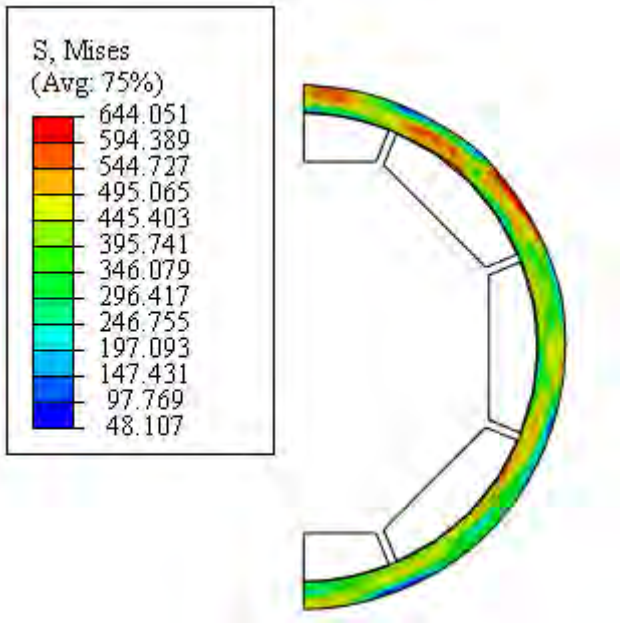

Figure 30: Numerical simulation of the UOE process ; Expansion.

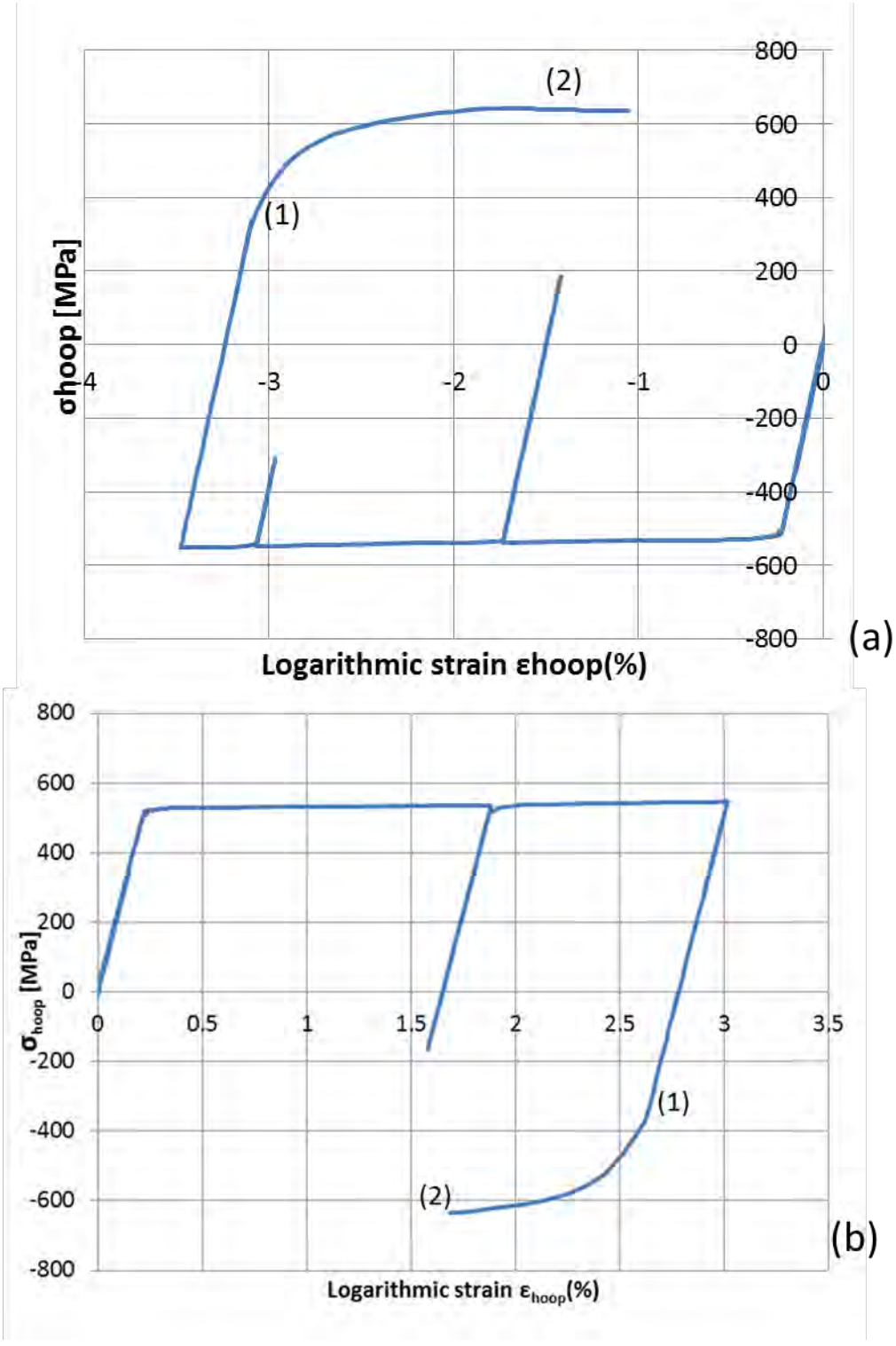

Figure 31: Stress-strain path at zero expansion at C.P.2: (a) interior surface; (b) exterior surface.

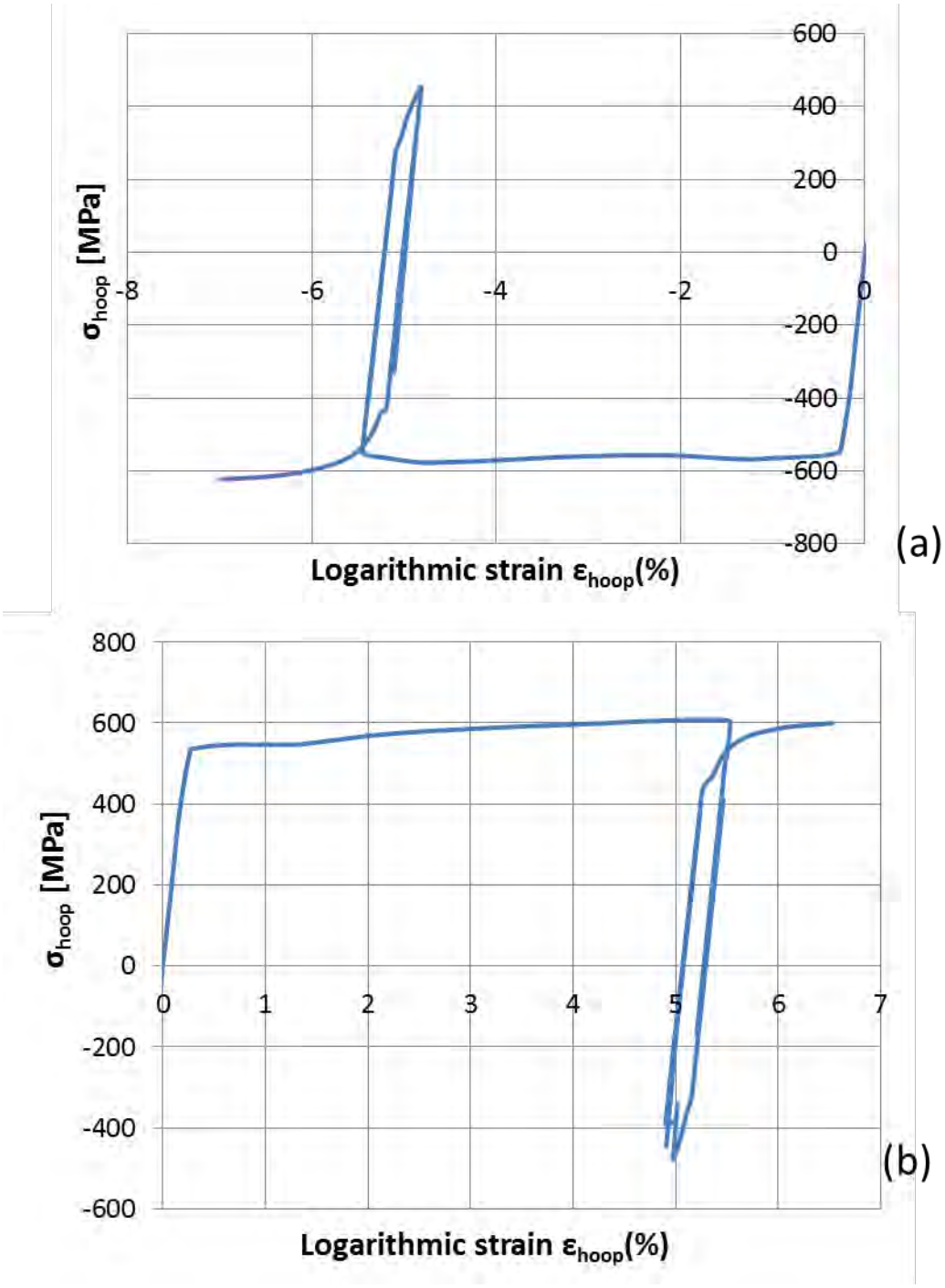

Figure 32: Stress-strain path at zero expansion at C.P.3: (a) interior surface; (b) exterior surface.

7 Effect of the UOE manufacturing process on pipeline structural performance

The installation of offshore pipelines in deep-water constitutes an important stage in underwater pipeline design procedure. There are several installation methods. For deep water pipelines, a common method for UOE pipes is the J-lay method (Figure 33). In J-lay method, high tension and relatively small external pressure occurs close to the surface of the sea, whereas the loading characterized by progressively increasing pressure and decreasing tension further down the long suspended section. On the other hand, high external pressure and bending exist in the sagbend, and essentially hydrostatic pressure is the loading condition on a flat seabed. Each of these loadings condition must be accounted for in the course of a pipeline mechanical design. In addition, in such deep waters, the possibility of accidentally initiating a propagating buckle cannot be overlooked, so that the installation of buckle arrestors becomes obligatory.

In the present study, the UOE pipe under consideration is subjected to loading conditions, which stem mainly from the installation procedure in deep water. In particular, external pressure loading and combined loading of bending and external pressure are considered.

(a)

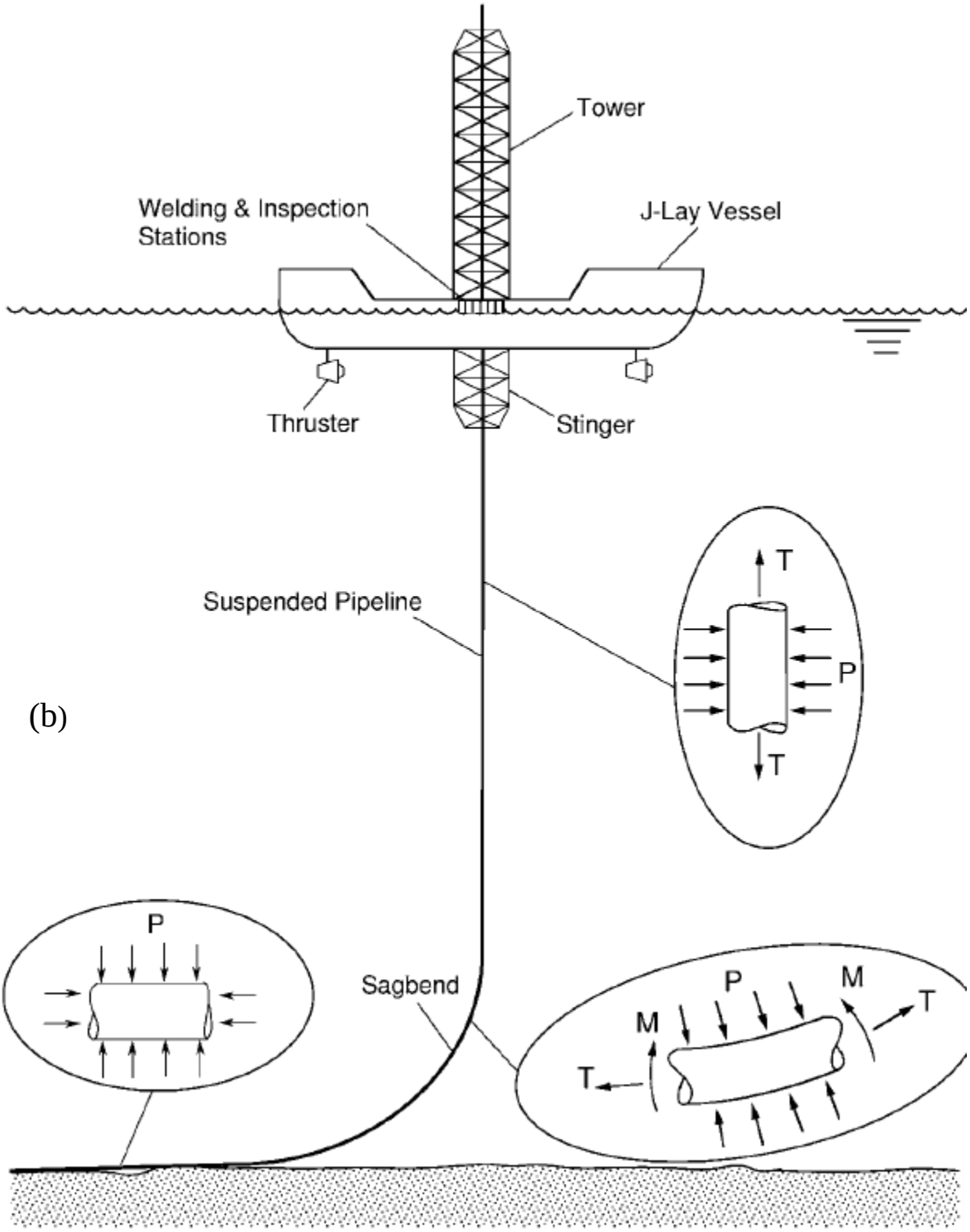

Figure 33: (a) Saipem 7000 semi-submersible crane vessel with a J-lay tower at its stern, (b)Pipe installation by J-lay method [22].

7.1 The effect of the UOE process on collapse pressure

The manufacturing process of UOE pipes affect the collapse pressure. The first major effect of the UOE process on the collapse pressure of the pipe refers to the ovalization of the pipe cross – section. During the forming process the steel pipe material experiences deformations far into the plastic range leading to residual stresses, which constitute a second parameter for the collapse pressure of the pipe. In the previous chapter, the stress – strain path in hoop direction in the middle of the pipe because of the UOE process and subsequent application of external pressure is illustrated. Due to UOE process and, subsequently, upon pressure application, ovalization occurs inducing plastic loading in the reverse direction, so that the Bauschinger effect is activated, as shown in Figure 31, resulting in premature yielding of the material. Such a stress-strain path cannot be simulated with a classical plasticity model (e.g. ISO or LKH).

The various expansion values that can be applied during the UOE manufacturing process may result in different collapse modes under external pressure loading. Figure 34 presents the cross-sectional configuration corresponding to zero expansion (u_E=0 mm), i.e. referring to a UO pipe, and to an expansion value equal to u_E=7.75mm (ε_E=1.00%). In the former case, the buckling shape (oval configuration) denoted as 0 is similar to the one in latter case, (denoted as ⬭), but it is rotated by 90º. The value of expansion at which transition from shape 0 to shape ⬭ occurs is equal to u_E=5.5 mm (ε_E=0.4%). In Figure 35 the collapse pressure P_{CO} is depicted in terms of the average circumferential permanent strain ε_E. It is important to note that as ε_E increases, the ovality initially drops sharply, as shown in Figure 24, causing P_{CO} to rise. Further increase of ε_E results to reduction of pipe ovality with a smaller rate and further decrease of the compressive material strength due to the Bauschinger effect. This results in a

maximum value of P_{CO} . Further increase of ε_E progressively reduces P_{CO}. As a result, there is an optimum expansion at which highest resistance in pressure loading is achieved. Herein, the optimum expansion strain is in the range of 0.35% to 0.45%, with the highest P_{CO} reached at 0.4%. It is also important to note that when ovalization is small (for induced permanent strain greater than 0.4%), the Bauschinger effect due to the manufacturing process is more pronounced, resulting in decrease of maximum collapse pressure. Figure 35 also shows that the present model predicts the same trend on the pressure capacity reported by Herynk *et al.*[17]. On the other hand, simulations conducted with isotropic and kinematic hardening plasticity models, similar to the ones reported in [18], [19], provided totally different results, mainly because these plasticity models are not capable at describing the Bauschingrer effect.

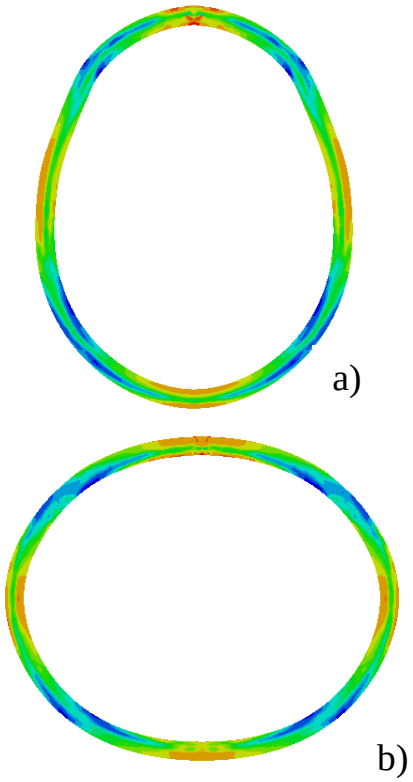

Figure 34: Configuration of pipe buckled cross-section under external pressure; (a) zero expansion (u_E =0 mm, UO pipe; mode shape), (b) UOE (u_E =7.75mm; mode shape).

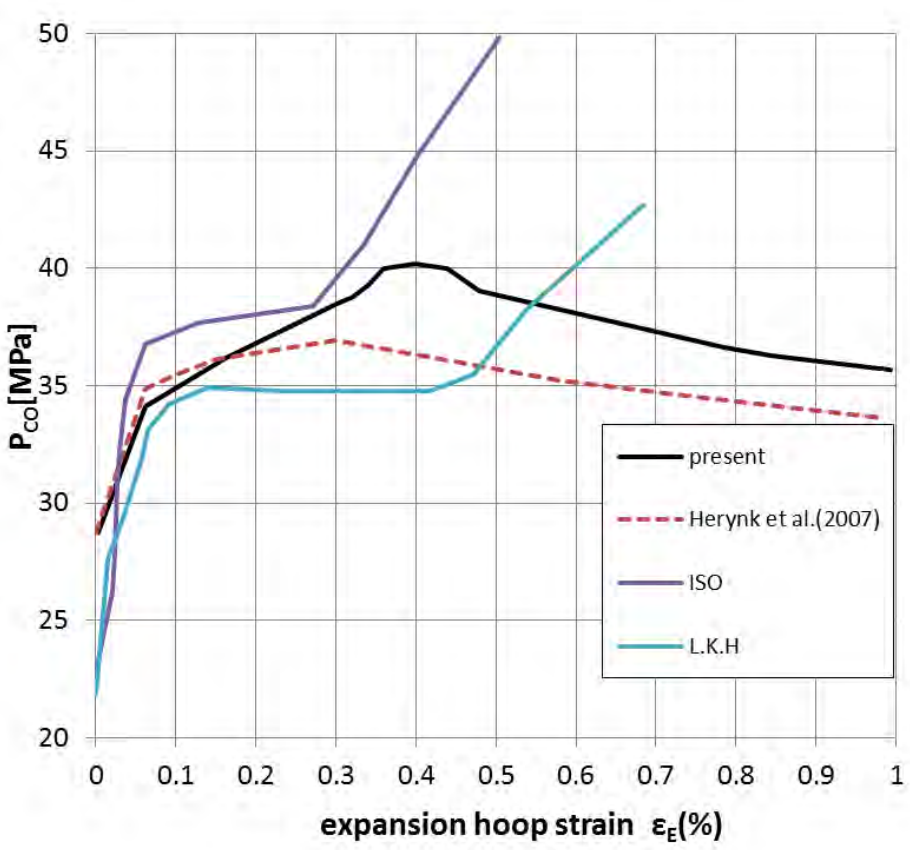

Figure 35: Variation of collapse pressure in terms of the permanent strain value ε_E.

For comparison purposes, the behavior of a seamless pipe with the same geometrical and material characteristics is also considered. Seamless pipes, because of their fabrication process, are known to have negligible residual stresses and strains and do not exhibit the Bauschinger effect. In Figure 36 the behavior of seamless pipe against external pressure is compared with the corresponding behavior of the UOE pipe, showing that seamless pipes have higher collapse pressure than UOE pipes for the same initial ovalization as noted by Gresnigt et al. [15] and Herynk et al. [17]. The cold forming process, and in particular the final cold expansion improves the tensile circumferential strength but decreases the compressive strength, due to the Bauschinger effect, and this parameter influences the collapse pressure.

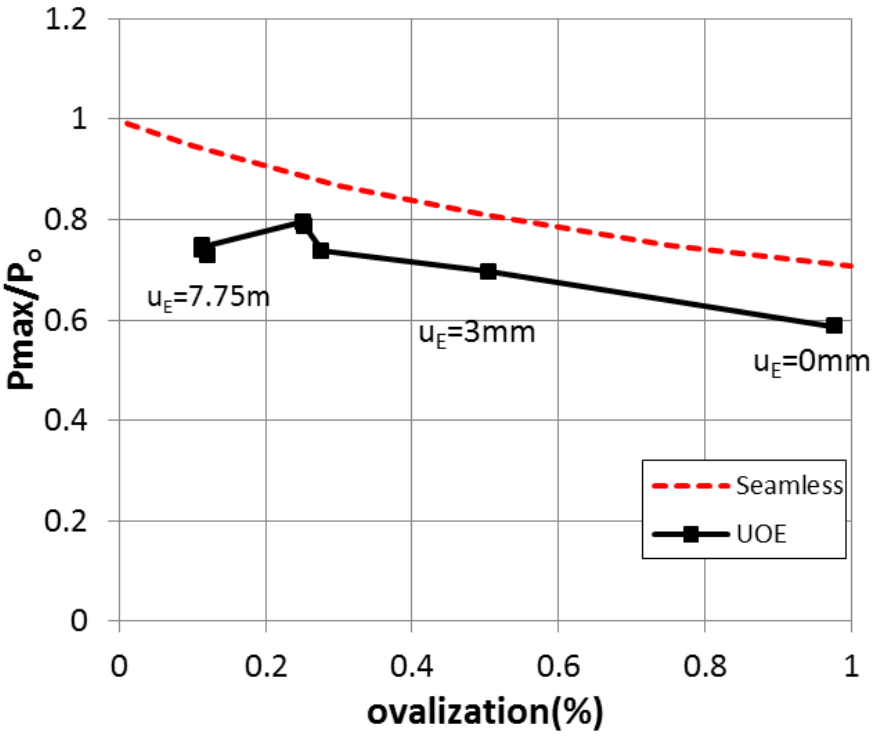

Figure 36: Collapse pressure and ovalization for UOE and Seamless pipes.

7.2 The effect of the UOE process on bending capacity

In the present section, the effect of UOE process on bending capacity in the presence of external pressure is examined, it is important to note that the critical curvature for collapse also depend on the sequence of loading, first pressure and then bending will give a different result than the other way round. The pipes are first subjected to a certain level of uniform external pressure load and subsequently, keeping the pressure constant, bending moment is applied until the pipe reaches the maximum moment. The curvature corresponding to this maximum moment is denoted as $k_{\max}$ and is the curvature of interest. The values of pressure P, moment M, and curvature $k_{\max}$ normalized by: $P_0 = 2\sigma_Y \, t/D_m$, $M_0 = \sigma_Y D_m{}^2 t$ and $k_1 = t/D_m{}^2$ respectively, where D_m is the mean pipe diameter, equal to $D_m = D - t$. Figure 37

illustrates the effect of expansion on the bending capacity in the presence of pressure at two levels, namely, $P / P_0 = 0.38$ and $P / P_0 = 0.19$. It is observed that the ultimate curvature capacity reduces as ε_E increases for significant values of expansion greater than 0.4%. For the case under consideration, a reduction equal to about 10% is observed when the ε_E increases from the value of ε_E=0.4% (u_E =5.5mm) to ε_E=1.0% (u_E=7.75mm). Figure 38 shows the moment–curvature diagrams for three characteristic values of expansion, namely ε_E=0.4% (u_E=5.5mm), ε_E=0.79% (u_E=7.0mm) and ε_E=1.0% (u_E=7.75mm).

The UOE manufacturing process introduces strains in the pipe body which are in the strain hardening region of the material, resulting to increased yield strength. This is beneficial for the bending capacity but the external pressure will cause compressive stress, and Baushinger effect becomes important, with negative effect in structural capacity. On the contrary, the corresponding seamless pipes do not undergo such a manufacturing process. Consequently they exhibit lower initial yield strength but not suffer from the Bauschinger effect. The effect of manufacturing process on the pressure-curvature interaction curve is depicted in Figure 39. The UOE(1) curve refers to the case where the applied bending moment results in tensile stresses at the weld region, while the UOE(2) curve refers to the opposite bending loading direction. As shown in Figure 39, the UOE pipe response is similar in both cases. The seamless pipe has the same geometrical characteristics with the UOE pipe and its steel material is similar to the material of the steel plate (σ_y=460MPa).

Figure 40 shows the moment–curvature curves for seamless and UOE pipe ($P / P_0 = 0.38$). The UOE pipe has a significantly different behavior compared to the seamless pipes. For small values of applied pressure, the UOE pipe is capable of reaching higher curvatures than the seamless pipe. As the pressure level increases, the resulting ultimate curvature is lower

than the one of the seamless pipe. The latter is attributed to the fact that the UOE pipe has a significant reduction in pressure capacity compared with the seamless pipe, also noted by Gresnigt and Van Foeken [15]. On the other hand, there is a beneficial effect on the ultimate bending capacity of the UOE pipe compared with the seamless pipe in terms of the ultimate curvature [23].

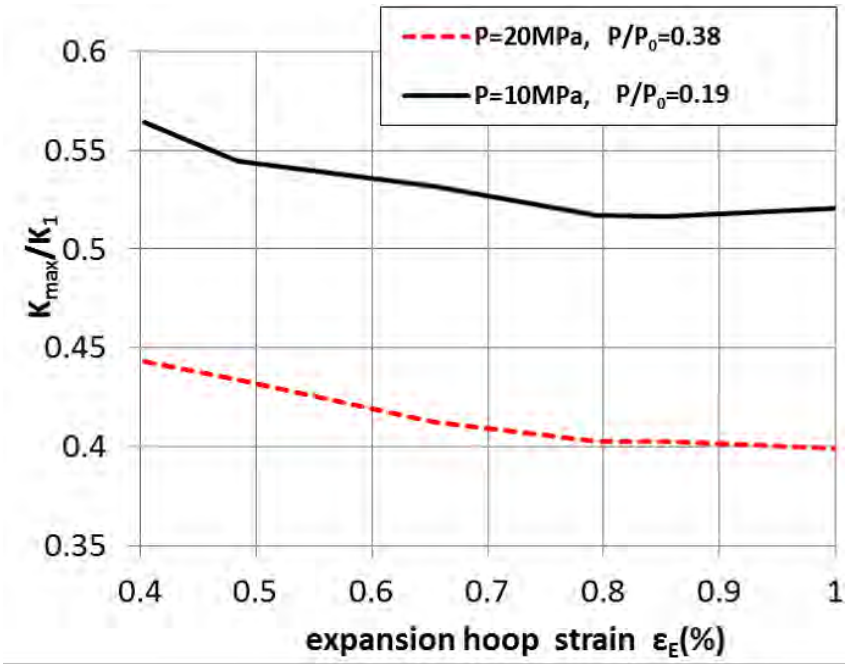

Figure 37: Variation of UOE collapse curvature in terms of permanent strain ε_E under to levels of external pressure.

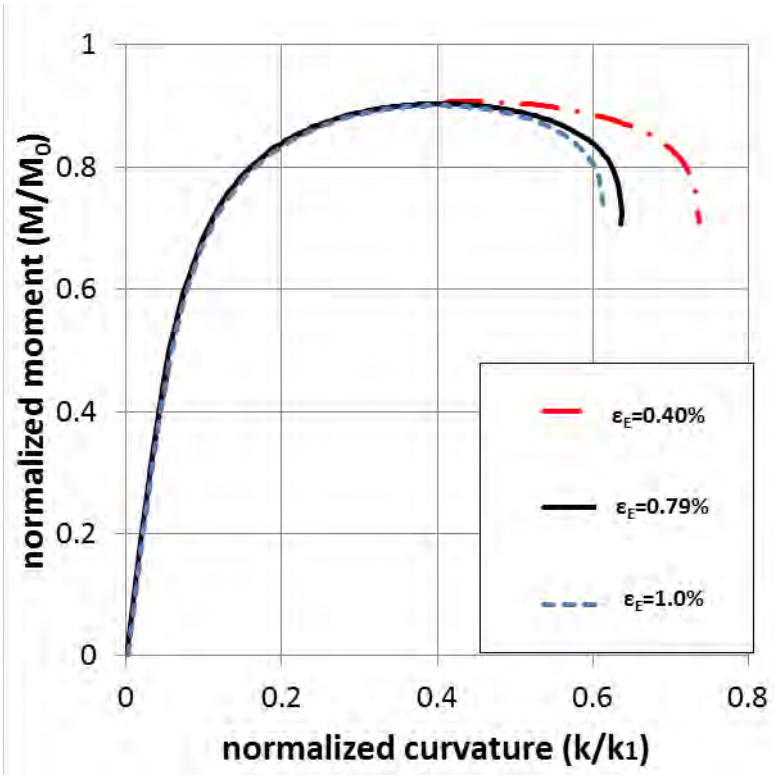

Figure 38**:** Moment–curvature interaction in the presence of external pressure, $P / P_0 = 0.38$ for three different expansion hoop strains.

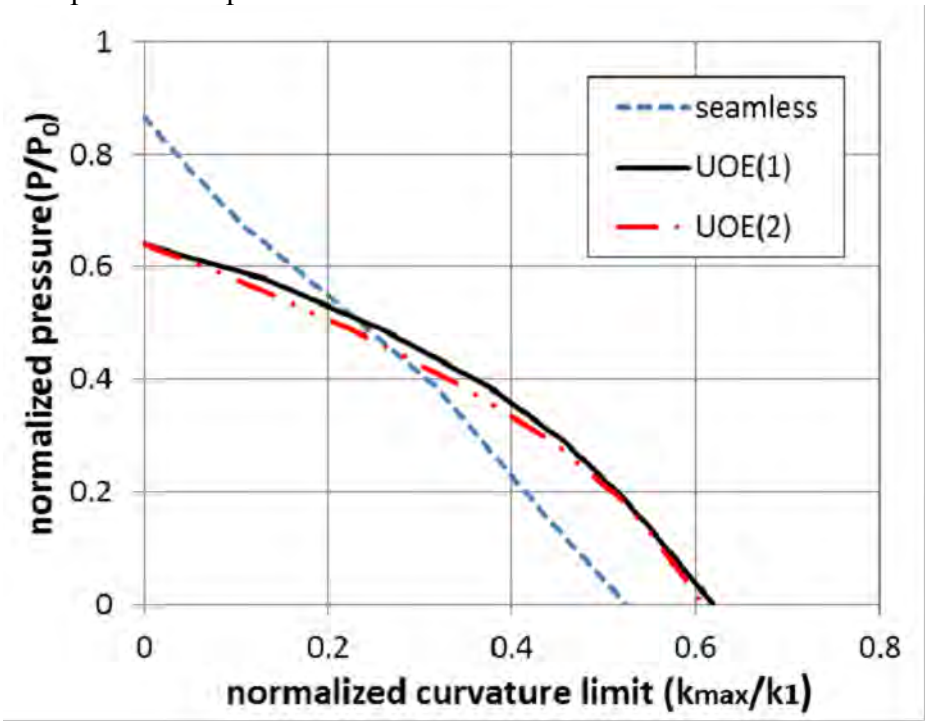

Figure 39: P-k for seamless pipes, UOE with positive and negative bending.

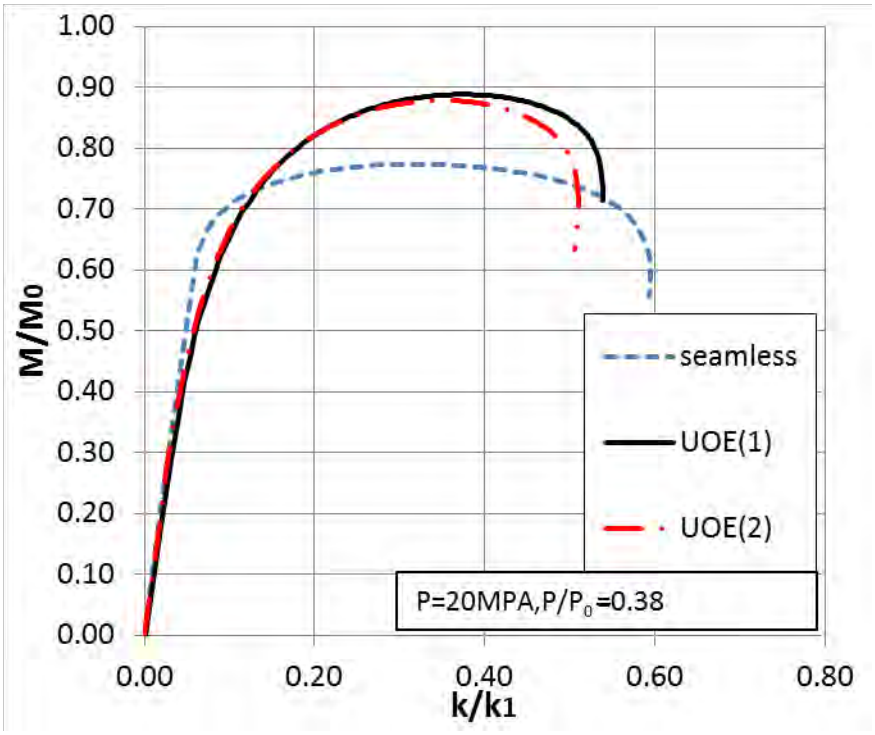

Figure 40: moment–curvature curves for UOE and seamless pipe.

7.3 Simplified analysis for pressurized bending response

The effect of UOE line pipe manufacturing process on the bending response of externally-pressurized thick-walled pipes is also examined, with an alternative methodology which uses more conventional finite element simulation tools. This constitutes an important step, because the simulations described in the previous sections require knowledge of the plate properties, the forming parameters, and other details that are not available to a design engineer. This complexity prompted the development of an approximate scheme for establishing the collapse loads of as-received UOE pipe under combined bending and pressure. The UOE forming process introduces significant changes in the stress–strain responses. To account for the state of deformation and stress upon ending of UOE process it is necessary to obtain two strip specimens in the longitudinal and in hoop direction of the pipe and obtain the corresponding stress- strain curves. In view of such experiments this is performed numerically. In particular, two integration points near the positions of the actual specimens (at 180º from weld) are

selected, and the state variables locked into these points are recorded. Considering a "unit cube" with those state variables, residual stresses are reduced to zero, and subsequent each point is loaded to a uniaxial compression strain of 1.0% in the circumferential direction and tension in axial direction. Those responses represent the mechanical behavior of those locations at each direction. The predicted stress–strain responses are plotted in

Figure 42, Figure 43. The yield stress in the hoop direction is lower indicating anisotropy of the yield surface, and the shapes of the two responses are also somewhat different. In the present analysis it is decided that the axial response to represent the fundamental response of the material, and the softer behavior in the circumferential direction is introduced by an anisotropy parameter S defined as follows

$$S = \frac{\sigma_{o\theta}}{\sigma_{o\chi}}$$

where $\sigma_{o\chi}$ is the yield axial stress and $\sigma_{o\theta}$ is the circumferential responses of the pipe in the same strain with the yield axial strain. For the case which is examined, *S* is equal to 0.908 according to the curve in Figure 43. This procedure is used to generate the anisotropy and the material parameters for the pipes. A pipe with the same geometrical characteristics (ovalization) and these material characteristic is considered, and these parameters were used to generate a $\mathrm{P} \rightarrow \mathrm{k}$ collapse envelope. The model used in this analysis is half-circular model (Figure 41), with the nominal geometric characteristic of the pipe, an anisotropic yield function plasticity model (Hill's yield surface) with isotropic hardening, calibrated through the axial stress-strain curve. For the radial direction two cases are considered, in first case [simplified method (1)] the radial yield stress is the same with axial, and in the second case [simplified method (2)] the radial yield stress is same with the circumferential Figure 44 illustrates that the results from such an analysis and show that it can provide very reliable results compared to the full simulation analysis of UOE line pipe manufacturing process

described in the previous section. Moreover, the anisotropy in radial direction is not important for the pressurized bending response.

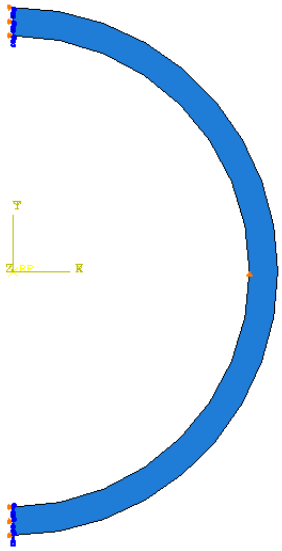

Figure 41: Schematic representation of the numerical model.

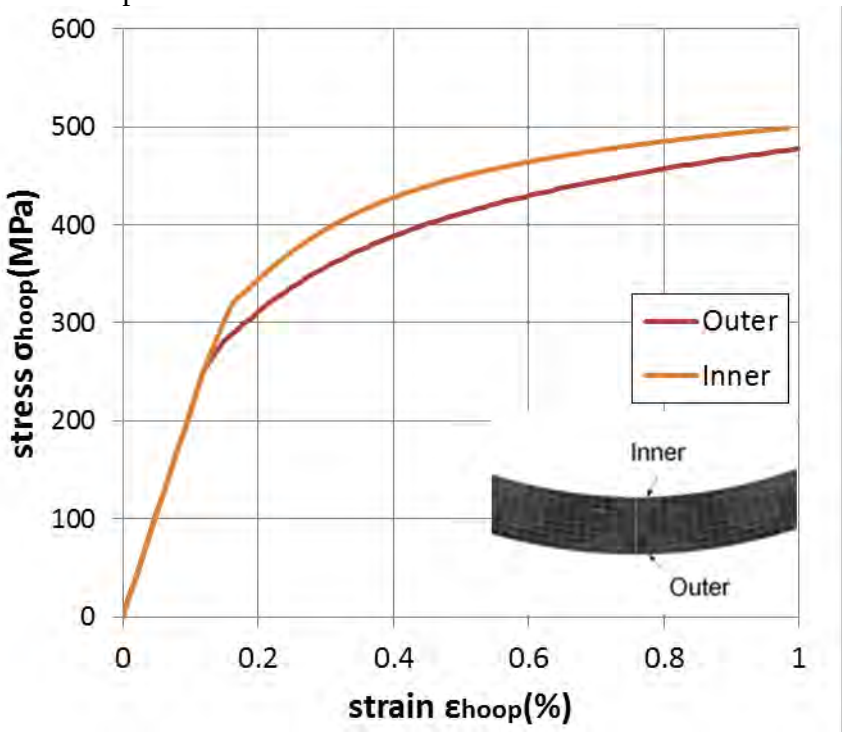

Figure 42: Compressive stress– strain responses in hoop direction at two locations through the pipe cross section.

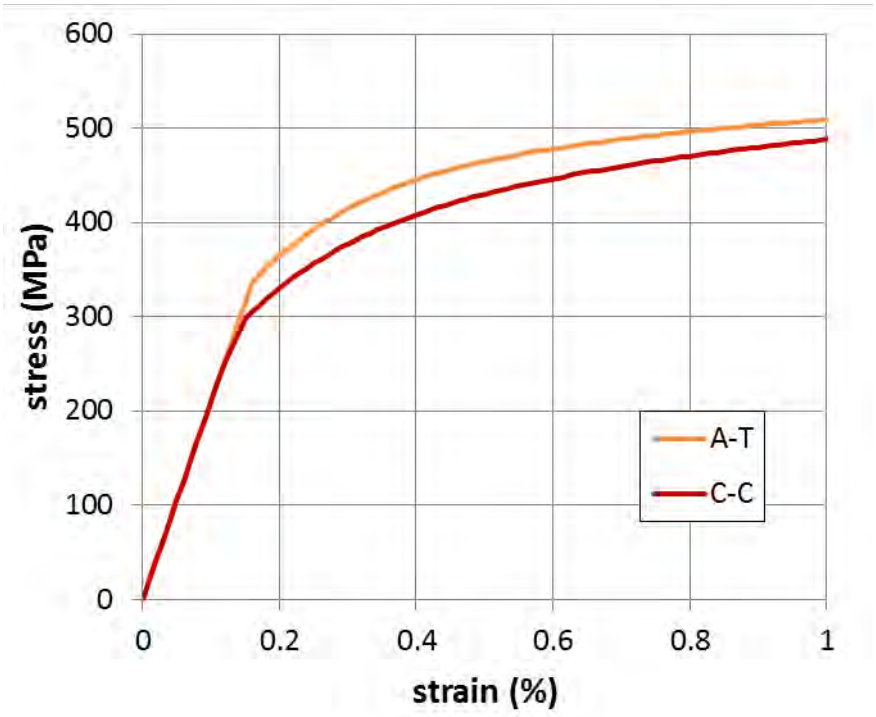

Figure 43: Comparison of the average axial tensile and compressive circumferential responses.

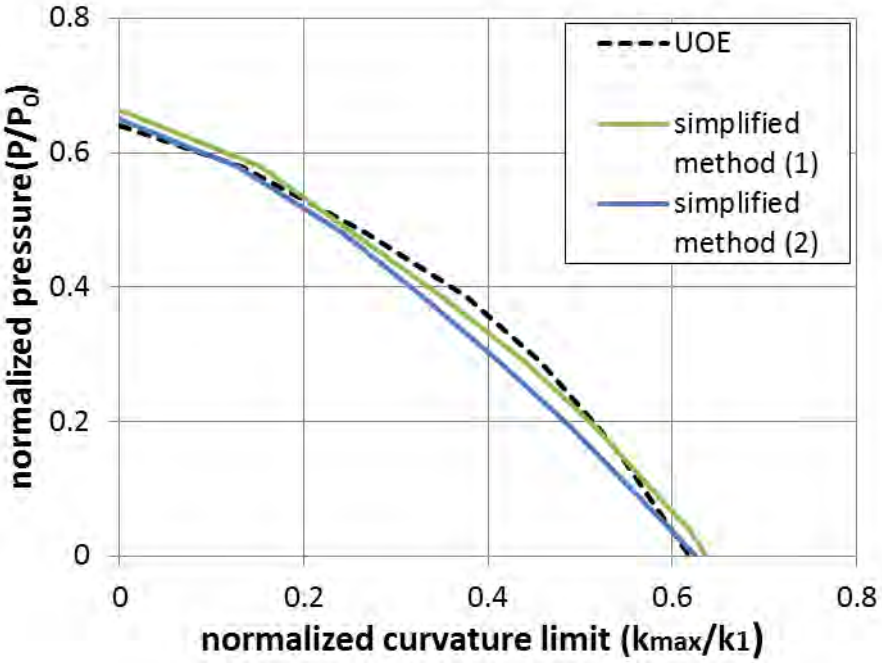

Figure 44: Comparison of UOE simulation to Simplified Method.

8 Conclusions

The UOE manufacturing process has been studied using nonlinear finite element simulation tools. In particular, an advanced plasticity model, capable of describing the nonlinear elastic–plastic material behavior, is adopted and implemented in the finite element model. The UOE manufacturing process steps are simulated and a parametric analysis is conducted focusing on the effects of the amount of expansion on the overall pipe behavior against pressure and bending loads. The analysis is based on a 24-inch-diameter pipe with D/t equal to 18.85 and showed that the increase of the total expansion value leads to minimization of the pipe out-of-roundness, but increases the Bauschinger effect, and consequently, reduces the collapse pressure resistance of the pipe. As a result, there exists an optimum expansion at which highest resistance in pressure loading is achieved. For combined pressure-bending loading conditions, and for relatively low external pressure levels, UOE pipes exhibit higher bending deformation capacity compared to seamless pipes. On the contrary, as the pressure level increases, UOE pipes are less resistant to bending loads. The developed numerical simulation is able to describe the effects of UOE manufacturing process on the overall structural behavior of the pipe and can be a powerful tool for identifying the values for the manufacturing parameters that optimize pipe performance in terms of pressure and bending load capacity. Finally, a simplified method is described that considers the material anisotropy of UOE pipes in the circumferential and in axial direction, capable at predicting the bending capacity with a good level of accuracy.

REFERENCES

[1] Stark P.R., McKeehan D.S, 1995. ‘‘Hydrostatic Collapse research in support of the Oman India gas pipeline ’’, Offshore Technology Conference (OTC 1995), Houston,Texas.

[2] Langner, C.G., 1984. “Design of Deepwater Pipelines”, 30th Anniversary Symposium on Underwater Technology, TNO-IWECO, Kurhaus, The Hague, The Netherlands.

[3] Yeh, M.K. and Kyriakides, S., 1986. “On the collapse of inelastic thick-walled tubes under external pressure”, Journal of Energy Resources Technology, Transaction of the ASME, Vol. 108 (1), pp. 35-47. MAR

[4] Karamanos, S.A. and Tassoulas, J.L., 1991. ‘‘Stability of Inelastic Tubes Under External Pressure and Bending’’, J. Engineering Mechanics, ASCE, vol. 117, no. 12, pp. 2845-2861.

[5] Kyriakides, S. and Yeh, M. K. 1985 . Factors affecting pipe collapse. Final report to American Gas Association, Project PR-106-404. Also, University of Texas at Austin, Engineering Mechanics Research Laboratory Report No. 85/1.

[6] Al-Sharif A. M., and Preston R., 1996 "Simulation of Thick walled Submarine Pipeline Collapse under Bending and Hydrostatic Pressure," Offshore Technology Conference (OTC 1996), Houston,Texas, p. no OTC 8212.

[7] Baek J.H., 2011 "Effect of Ovality and Eccentricity on Collapse Pressure of Subsea Pipeline," International Gas Union Research Conference, Ansan, Korea, p.no IGU2011-P2-34.

[8] Benjamin A. C., and Cunha, D. J. S., 2012, "Assessment of Hydrostatic Collapse of Submarine Pipelines: Historical Review of the Classic Methods," 9th International Pipeline Conference (IPC2012), Calgary, Canada, p. no IPC2012-90617.

[9] DeGeer D., and Cheng J. J., 2000, "Predicting Pipeline Collapse Resistance," International Pipeline Conference, Alberta, Canada, p. no IPC 00-0168.

[10] Guarracino F., Fraldi M., Freeman R., and SlaterS, 2011, "Hydrostatic Collapse of Deepwater Pipelines: A Rigorous Analytical Approach," Offshore Technology Conference (OTC 1996), Houston, Texas, p. no OTC 21378.

[11] Haagsma S. and Schaap D., 1981 "Collapse resistance of submarine lines studied," Oil and Gas Journal, 79 (5), pp. 86-90, 1981.

[12] Murphey C. E. and Langner C. G., 1985, "Ultimate Pipe Strength under Bending, Collapse and Fatigue," Proceedings of the 7th International Conference on Offshore Mechanics and Arctic Engineering (OMAE 1985).

[13] Tsuru E. and Asahi H., 2004, "Collapse Pressure Prediction and Measurement Methodology of UOE Pipe," International Journal of Offshore and Polar Engineering, 14 (5), pp. 51-59

[14] Corona E., and Kyriakides S., 1988. “On the collapse of inelastic tubes under combined bending and pressure. Intl J. Solids Struct. 24, 505–535.

[15] Gresnigt A.M, Van Foeken R.J, Chen SL , 2000. "Collapse of UOE Manufactured Steel Pipes," Proceedings of the Tenth International Offshore and Polar Engineering Conference (ISOPE), Seattle, May 28 - June 2, 2000, Vol. II. pp. 170-181..

[16] Kyriakides S.,Corona E., Fischer F.J., 1991. ‘‘On the Effect of the UOE Manufacturing Process on the Collapse Pressure of Long Tube’’, Proceedings of 23th Offshore Technology Conference, pp. 531-543 Houston, Texas, USA.

[17] Herynk M.D., Kyriakides S., Onoufriou A., Yun H.D., 2007. “Effects of the UOE /UOC pipe manufacturing processes on pipe collapse pressure”, International Journal of Mechanical Sciences, vol. 49, pp. 533–553.

[18] Toscano R.G., Raffo J., Fritz M., Silva R.C., Hines J., TimmsC., 2008. “Modeling the UOE Pipe Manufacturing Process”, Proceedings of 27th International Conference on Offshore Mechanics and Arctic Engineering, OMAE2008-57605, Estoril, Portugal

[19] Varelis G. E., Vathi M., Houliara S., Karamanos S. A., 2009. ‘‘Effect of UOE Manufacturing Process on Pressure Buckling of Thick-Walled Pipes’’, X International Conference on Computational Plasticity, CIMNE, Barcelona.

[20] Armstrong, P.J., Frederick, C.O., 1966. “A mathematical representation of the multiaxial Bauschinger effect”, CEGB Report No. RD/B/N 731.

[21] Ucak, A. and Tsopelas, P., 2011. “Constitutive Model for Cyclic Response of Structural Steels with Yield Plateau”, Journal of Structural Engineering, ASCE, pp. 195-206.

[22] Kyriakides, S. and Corona, E., 2007.”Mechanics of offshore pipelines”, Collapse. Elsevier.

[23] Gresnigt A.M, Van Foeken R.J., 2001. ‘‘Local Buckling of UOE and Seamless Steel Pipes’’, Proceedings of the Eleventh International Offshore and Polar Engineering Conference, pp.131-142, Stavanger, Norway.

[24] ABAQUS v 6.10 Documentation - Analysis User’s Manual.

[25] Fernandes et al , 2013. “Small scale material tests on X52”,ULCF report.